Full-Scale Controlled Tests of Wind Loads on Traffic Signal Structures

Authors: Christopher Letchford, Hector Cruzado

Notice

1. Report No.: FHWA/TX -07-4586-3	2. Government Accession No.:	3. Recipient's Catalog No.:
4. Title and Subtitle: Full-Scale Controlled Tests of Wind Loads on Traffic Signal Structures		5. Report Date: May 2008
		6. Performing Organization Code:
7. Author(s): Christopher Letchford, Hector Cruzado		8. Performing Organization Report No. 0-4586- 3
9. Performing Organization Name and Address: Texas Tech University College of Engineering Center for Multidisciplinary Research in Transportation Box 41023 Lubbock, Texas 79409-1023		10. Work Unit No.
		11. Contract or Grant No. : Project 0-4586
12. Sponsoring Agency Name and Address Texas Department of Transportation Research and Technology Implementation P. O. Box 5080 Austin, TX 78763-5080		Type of Report and Period Cover: Technical Report August 2003-October 2007
		14. Sponsoring Agency Code:
15. Supplementary Notes: Project performed in cooperation with the Texas Department of Transportation and the Federal Highway Administration. Revision of AASHTO Fatigue Design Loadings for Signs, Luminaires and Traffic Signal Structures for Use in Texas		

16. Abstract:

The wind-induced vibrations of the mast arm of cantilever traffic signal structures can lead to the fatigue failure of these structures. For this project, both full-scale and wind tunnel tests were conducted to study the behavior of the structures. Results of these experiments indicated that when the signals have backplates, vortex shedding can cause large-amplitude vibrations that may lead to fatigue failure. These results contradict what has been generally accepted by other researchers: that galloping is the main cause for the fatigue inducing vibrations and that vortex shedding is of no relevance in this type of structure.

As a result of this research, a methodology to estimate the fatigue life of these structures was developed. Using the climatology of the region, the methodology was applied as a risk assessment model to traffic signal structures of the city of Lubbock. Guidance is given on how life-cycle cost analysis can be applied to the structures.

17. Key Words: Cantilever, mast arm, galloping, fatigue failure, vortex shedding, backplates	Distribution Statement – No restrictions. This document is available to the public through the National Technical Information Service, Springfield, VA 22161 www.ntis.gov		
19. Security Classif. (of this report) Unclassified	20. Security Classif. (of this page) unclassified	21. No. of Pages 54	22. Price

Full-Scale Controlled Tests of Wind Loads on Traffic Signal Structures

by
Christopher J. Letchford
Hector Cruzado

Department of Civil and Environmental Engineering
Texas Tech University
Center for Multidisciplinary Research in Transportation

Research Report Number 0-4586-3
Research Project Number 0-4586
Revision of AASHTO Fatigue Design Loadings for Signs, Luminaires, and Traffic Signal Structures for Use in Texas

Report No. 0-4586-3   May   2008

AUTHOR'S DISCLAIMER

The contents of this report reflect the views of the authors who are responsible for the facts and the accuracy of the data presented herein. The contents do not necessarily reflect the official view of policies of the Texas Department of Transportation or the Federal Highway Administration. This report does not constitute a standard, specification, or regulation.

PATENT DISCLAIMER

There was no invention or discovery conceived or first actually reduced to practice in the course of or under this contract, including any art, method, process, machine, manufacture, design or composition of matter, or any new useful improvement thereof, or any variety of plant which is or may be patentable under the patent laws of the United States of America or any foreign country.

ENGINEERING DISCLAIMER

Not intended for construction, bidding, or permit purposes.

TRADE NAMES AND MANUFACTURERS' NAMES

The United States Government and the State of Texas do not endorse products or manufacturers. Trade or manufacturers' names appear herein solely because they are considered essential to the object of this report.

TABLE OF CONTENTS

List of Tables

List of Figures

Executive Summary

Full-scale experiments have been conducted with two cantilever traffic signal structures at the facilities on Texas Tech University. One signal has a 60-ft. long arm, while the other is 44-ft. long. Each structure was instrumented with a sonic anemometer mounted above the mast together with a video camera monitoring the motion at the top of the cantilever arm. The camera tracks the motion of an infrared target. Data is acquired at 30 Hz.

Results of data collected for the structures having signals with backplates indicate that, conventional theories to the contrary, vortex shedding is a significant cause of mast arm vibrations. The findings of this study include the observation that the largest amplitude vertical oscillations have a higher probability of occurring when the wind speed is steady between 5 and 10 mph, which combined with the backplate vertical dimension, gives a Strouhal number of -0.1. This is a characteristic of vortex shedding from this shape. It also appears that the vibrations are more likely to occur when wind approaches the arm from behind the signal.

Experimental Setup

Two out-of-service cantilever traffic signal structures were tested at the Reese Technology Center facilities of the Wind Sciences and Engineering Research Center of Texas Tech University. These structures are shown in Figure 1.

Figure 1. Two Cantilever Traffic Signal Structures Tested at Reese Technology Center

Foundations

Each structure rests on a foundation that allows the whole mast/arm assembly to be rotated in 15" increments of direction. Each foundation consists of a round steel plate on top of a reinforced concrete cylinder, as shown in Figure 2. For more details on the foundations, refer to Appendix A.

Figure 2. Foundation of Steel Plate Allowing Rotation of Mast/Arm Assembly

Geometry and Light Configuration

The major difference between the two structures tested is the length of their arms. Traffic signal 1 (TS1) has an arm length of 60 feet, while traffic signal 2 (TS2) has an arm length of 44 feet. Both TS1 and TS2 are fabricated from steel. TS1 supports one signal with five heads and three signals with three heads; TS2 supports one signal with five heads and two signals with three heads. More details of the geometry and light configuration of the structures for the case when signals have backplates are shown in Figures 3 and 4.
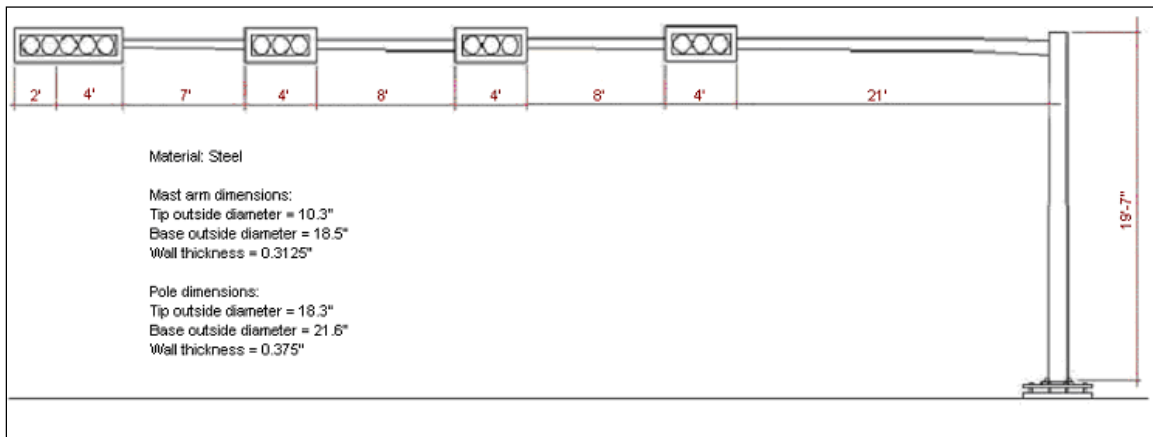

Figure 3. Geometry and Light Configuration of TS1 (60' mast arm)
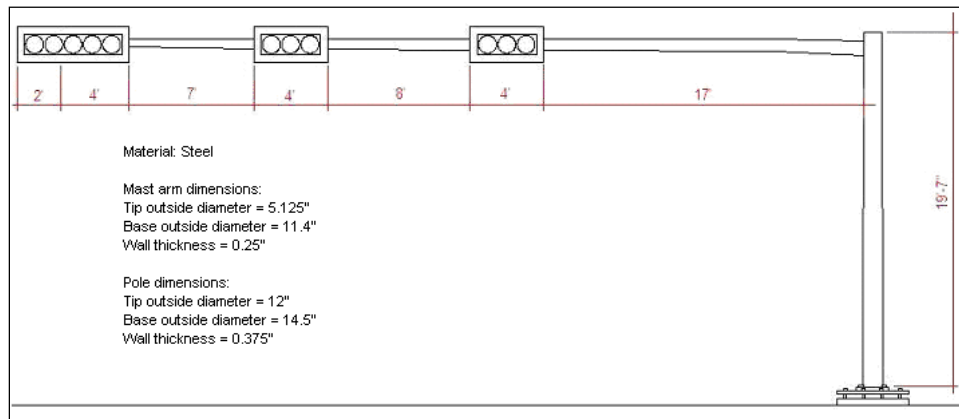

Figure 4. Geometry and Light Configuration of TS2 (44' mast arm)

<u>DAQ System</u>

Figure 5 shows a schematic layout of the instrumentation used to collect data for each structure. The instrumentation consists of the following:

- Infrared target made of two Nerlite S-40 infrared lights. The target is rigidly attached near the tip of the arm, as shown in Figure 6.

- Basler A601 video camera with National Instrument Compact Vision System (CVS) 1454 to collect displacement data. The camera and the CVS are placed inside a camera enclosure which is mounted on top of the mast, pointing towards the tip of the arm. The camera has a filter to capture only the two lights of the infrared target. The camera has a resolution of 0.12 inches at a distance of 60 ft from the target and is set for a sampling rate of 30 Hz. The position of each infrared light is collected and used to calculate the X and Y coordinate in pixels of the midpoint between the two lights. These instruments are calibrated by using the physical separation of the centers of the infrared lights (G Systems 2005). The instruments, along with the coordinates, also record calibration factors for each X and Y coordinates to change the values from pixels to inches. Other data that is collected by these instruments that was not used in this research is: radius in pixels and circularity factors for each of the infrared lights, angle in degrees for the segment between the infrared lights, calculated metric threshold value used in the image analysis, and cumulative image buffer number.

- R. M. Young Model 81000 ultrasonic anemometer mounted about 4 ft above the top of the pole. The anemometer measures three-dimensional wind velocity and is also sampled at 30 Hz. It collects u, v, and w wind components as voltages. The anemometer is oriented so that positive u and v are measured as shown in Figure 7, with w being the vertical component which is positive going upwards. Also show in Figure 7 is the angle of attack sign convention. The anemometers were calibrated by the manufacturer in a wind tunnel before data collection began and the calibration is usually good for two years. This instrument also records relative humidity and temperature, but this data was not used in this research.

- National Instruments FP-2000 Intelligent Ethernet Controller Interface for FieldPoint which gathers the data from the anemometer and the camera/CVS and sends it to a computer at the field site.
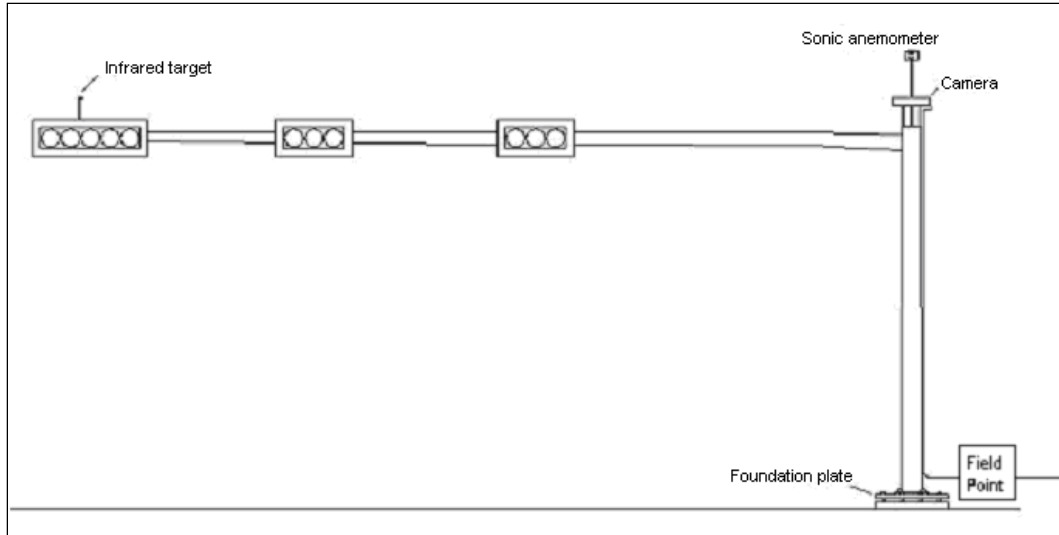
Figure 5. Instrumentation

Figure 6. Infrared Target, As Viewed from the Top of the Pole

5
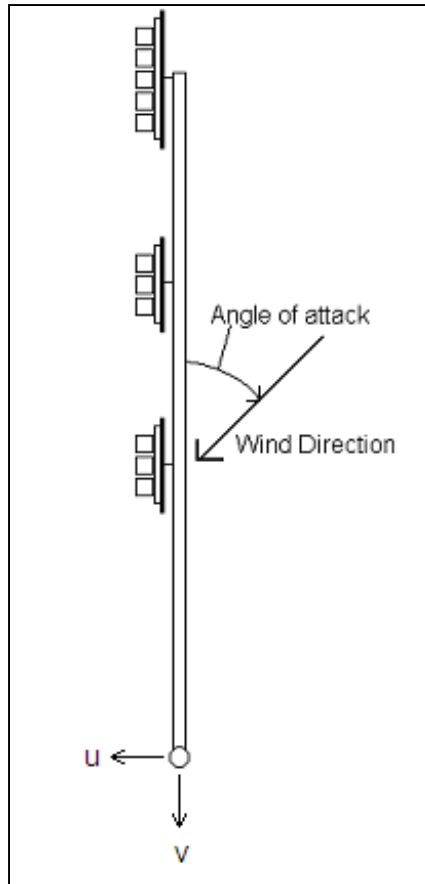
Figure 7. Anemometer Orientation and Angle of Attack Sign Convention

This DAQ system only measures the relative displacement of the top of the arm with respect to the pole. It does not take into account if there are any displacements of the tip of the pole. This research is chiefly concerned with the relative displacement because most significant fatigue failures occur at the arm, close to where it connects to the pole (Chen, et al; Cook et al; Gray et al; Hamilton, et al; Hartnagel and Barker; Pulipaka).

The field site computer has software developed by G Systems that is designed to save the data collected by four instruments:

1. The anemometer of TS1.
2. The camera/CVS of TS1.
3. The anemometer of TS2 and
4. The camera/CVS of TS2.

0-4586-3

The software starts recording data from all four instruments at the same time. One hour later, the software stops recording, saving a time history file for each of the four instruments, and one minute later starts data collection again. The file name convention is as follows:

M####_R####_DTmmddyy_TMhhmmss_TR_D##_HW_Platform.csv

where:

- M#### is MODE number. The number can be changed to describe different experiments.

- R#### is RUN number. The number automatically increases by one for each new run. One hour of data is a run.

- DT is the DATE of the run.

- TM is the TIME that the run file was created.

- TR is the indication that this is a run data file rather than another type of file such as calibration data.

- D## is the device number.

  - D01 = anemometer on TS1
  - D02 = CVS on TS1
  - D03 = anemometer on TS2
  - D04 = CVS on TS1

- HW is the hardware type: FP for anemometer data or CV for camera data.

- Platform is the platform type, in this case SIGNALLIGHT. (This software is used on other experiments, so those would have different platforms.)

It is noted here that the four data files recorded at the same time have almost the same name, but they can be differentiated by the device number and the hardware type.

Approximately once a week, the recorded data is taken from the field computer and saved on a server at the Wind Science and Engineering Research Center. There the data is processed with software developed at Texas Tech. This software groups the four hour-long files recorded at the same time into one file, changing the voltages collected by the anemometers and displacements to engineering unit (mph & in.) For the processed data, the file name convention is:

M####_R####_DTmmddyy_TMhhmmss

where:

- M#### is MODE number - the same mode number it had when the data was collected.

- R#### is RUN number - the same run number it had when the data was collected.

- DT is the DATE the data was processed.

- TM is the TIME the data was processed.

Each processed file has approximately 108,000 lines (1 hour collection at a 30 Hz sampling rate), but it has exactly 24 columns. Table 1 on the following page lists the content of each of the columns of processed files.

Table 1. Content of Each Column of Processed Files

Column No.	Content
1	Temperature of TS1 (Fahrenheit)
2	U velocity component for TS1 (mph)
3	V velocity component for TS1 (mph)
4	W velocity component for TS1 (mph)
5	X coordinate of the midpoint between infrared lights for TS1 (inches)
6	Y coordinate of the midpoint between infrared lights for TS1 (inches)
7	Calibration factor for X coordinate of TS1 (inches/pixels)
8	Calibration factor for Y coordinate of TS1 (inches/pixels)
9	Temperature of TS2 (Fahrenheit)
10	U velocity component for TS2 (mph)
11	V velocity component for TS2 (mph)
12	W velocity component for TS2 (mph)
13	X coordinate of the midpoint between infrared lights for TS2 (inches)
14	Y coordinate of the midpoint between infrared lights for TS2 (inches)
15	Calibration factor for X coordinate of TS2 (inches/pixels)
16	Calibration factor for Y coordinate of TS2 (inches/pixels)
17	Wind velocity for TS1 (mph)
18	Wind direction for TS1 (mph)
19	Along-wind velocity component for TS1 (mph)
20	Cross-wind velocity component for TS1 (mph)
21	Wind velocity for TS2 (mph)
22	Wind direction for TS2 (mph)
23	Along-wind velocity component for TS2 (mph)
24	Cross-wind velocity component for TS2 (mph)

9

Quality Assurance Measures

To assure the data collected by the anemometers on the traffic signals was of good quality and that it was processed correctly, data from the West Texas Mesonet station located at Reese Technology Center was used for comparison at various times. This station is located less than 1,500 feet from each of the signals' foundations. Figure 8 is an example of such a comparison for a random hour of data collected. The anemometer data at TS1 and TS2 have been used to calculate time histories of wind direction and these were compared to data collected by the West Texas Mesonet.
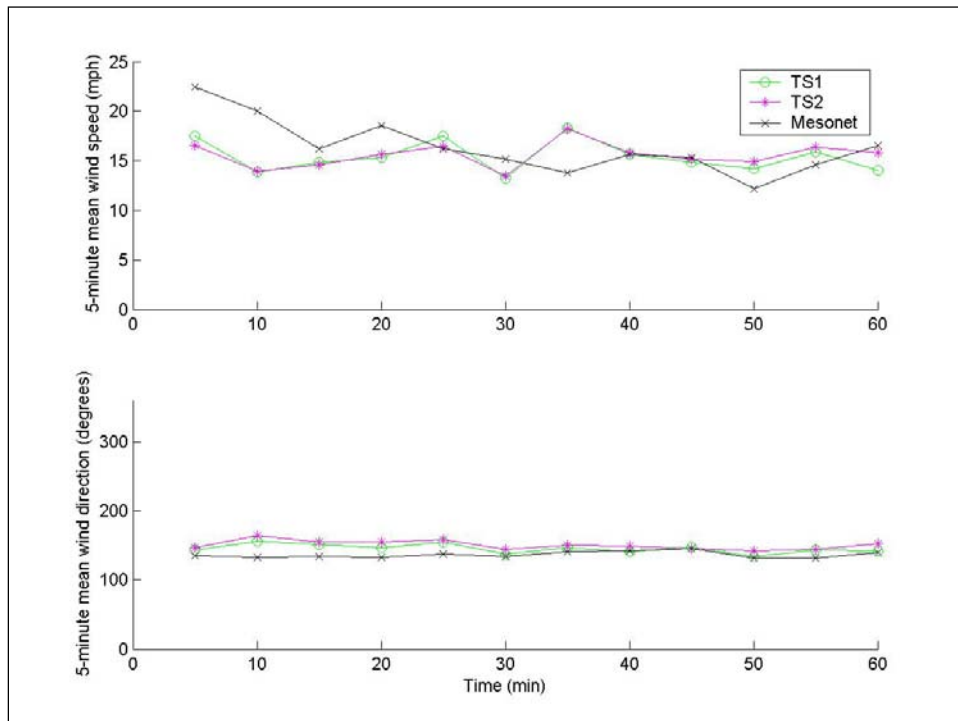

Figure 8. Comparison between Data Collected by the Traffic Signals' Anemometer and the West Texas Mesonet Site at Reese Technology Center

To monitor the quality of the data collected by the camera/CVS, the time history of the X and Y coordinates of the two infrared lights was used to calculate a time history of the distance between the two infrared lights of each hour-long file. This calculated distance should remain close to constant, since the actual distance of the lights never varies. Figure 9 shows an example of a comparison being made. Notice that the calculated values show little variability and they remain fairly close to the actual value. Using the time history of the calculated distance, an average value was computed. If a run had an average value with an error of more

10

than 1.5 %, then the run was not considered of good quality and it was not used for analysis of results.
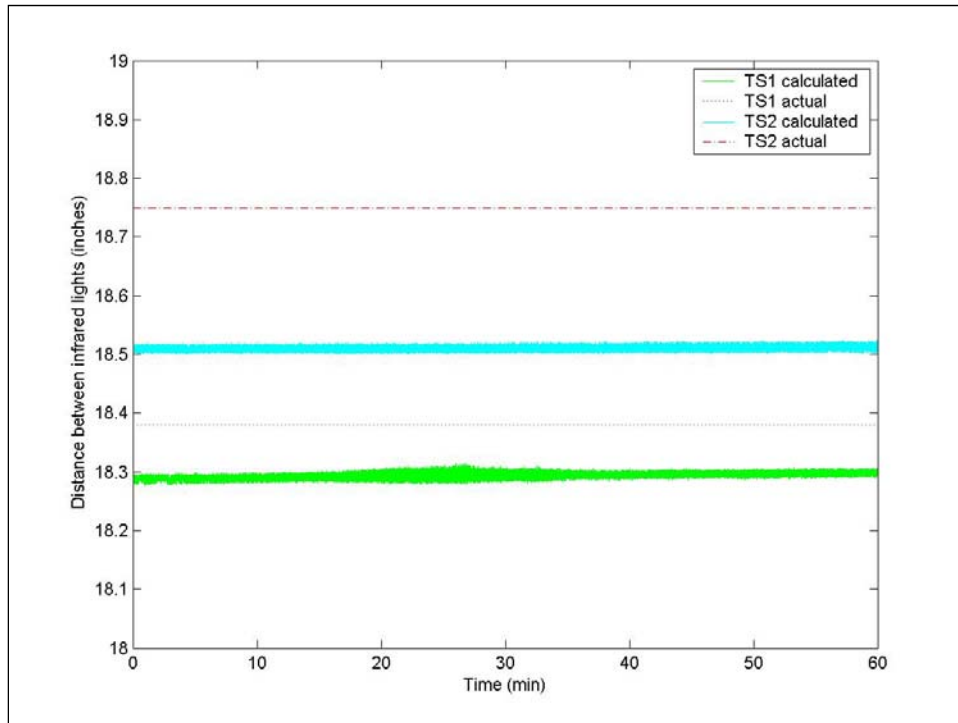

Figure 9. Comparison between Actual and Calculated Distances between Infrared Lights

Experimental Program

Initially the traffic signals were set up at the Reese site with the arm pointing east (the camera is also pointed east) to take advantage of the predominant north-south winds in the area. Although some interesting significant data was collected under these conditions, there were problems with the camera recording data during sunrise. A decision was made to change the structure to have the arm pointing north.

Mode 1100 was designated as the experimental setting of the arm's traffic signals pointing north and <u>with</u> backplates on the signals. Mode 1101 indicated the experimental setting of the arms pointing north <u>without</u> backplates on the signals. Data was collected under Mode 1100 from April 2002 to March 2006. Data from Mode 1101 was collected starting in March 2006 and continuing through February 2007. Other possible modes to collect data in the future would include signals with vented backplates, with damping plate and other configurations deemed necessary to complete the experimental matrix.

<u>Pluck Test</u>

A pluck test was conducted to determine the fundamental frequencies and the damping ratios of the arms of the structures at the Reese site. The tests were conducted by pulling and pushing the tip of the arm in either the horizontal or the vertical direction and then letting the arm vibrate freely until it stopped. There were a total of four cases tested:

1. Horizontal vibrations of 60-ft arm,

2. Vertical vibrations of 60-ft arm,

3. Horizontal vibrations of 44-ft arm, and

4. Vertical vibrations of 44-ft arm.

For each of the four cases, three runs were conducted. While conducting the runs, the instrumentation recorded a time history of the displacement. Figure 10 is an example of a plotted time history of one run for the case of the 44-ft arm with horizontal vibrations after it had already been excited and left to vibrate freely. This history has a length of 56.13 seconds, and it can be seen from the figure that 50 cycles of motion were completed, so the fundamental frequency was calculated as:

$$f_o = \frac{50}{56.13} = 0.89 \text{ Hz} \qquad\qquad \text{Equation 1}$$

The damping ratio is determined by using the Logarithmic Decrement method (Paz 2002), which in Figure 10 is represented by the red curve. Knowing that the curve should be given by:

$$X = A \exp(-\zeta \, \omega_o \, t) \qquad\qquad \text{Equation 2}$$

in which ζ is the damping ratio and t is the time. Therefore, for the case of Figure 10, the damping ratio is calculated as:

$$\zeta = \frac{0.028}{2\pi \, f_o} = \frac{0.028}{2\pi(0.89)} = 0.50 \text{ \%} \qquad\qquad \text{Equation 3}$$
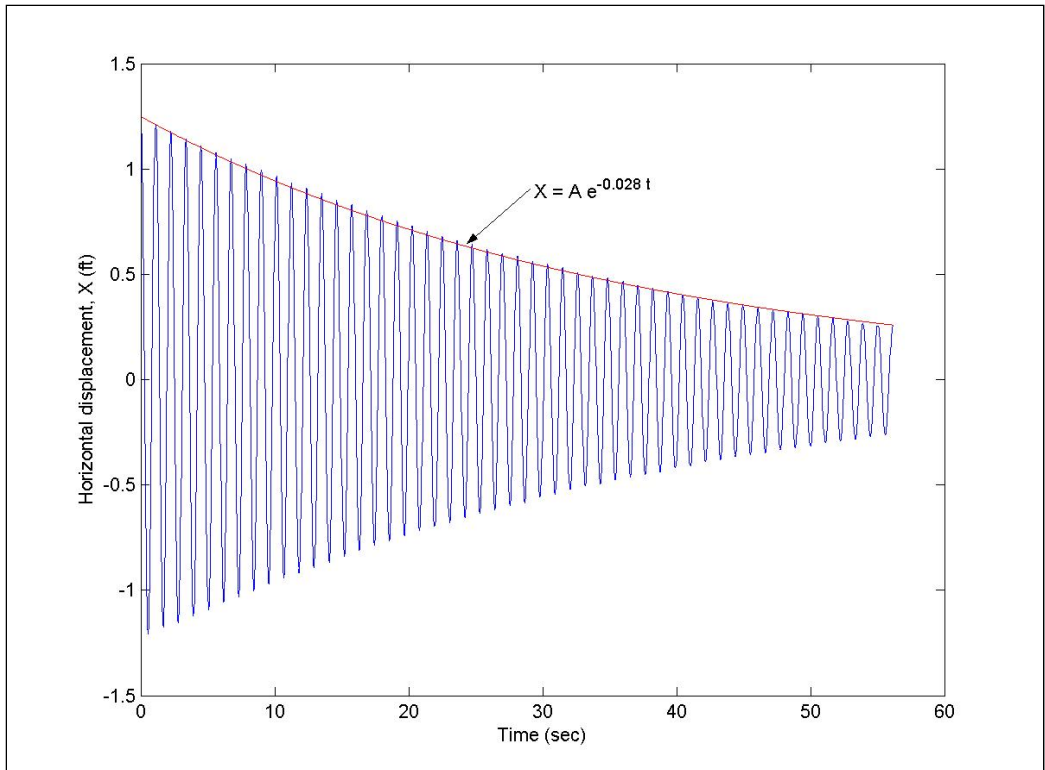
Figure 10. Pluck Test Run for Case of 44-ft Arm under Horizontal Vibrations

The results obtained for the three runs were used to calculate average values for each case. The resulting average values are presented in Table 2.

Table 2. Fundamental Frequency (f_o) and Damping Ratio (ζ) of Mast Arms

		Mast Arm Length	
		60 ft	44 ft
f_o			
	Horizontal	0.92 Hz	0.89 Hz
	Vertical	0.98 Hz	0.98 Hz
ζ			
	Horizontal	0.25 %	0.55 %
	Vertical	0.23 %	0.28 %

Displacement-Stress Relationship

For sinusoidal motion, the amplitude A can be calculated as:

$$A = \sqrt{2}\sigma_{rms} \qquad\qquad \text{Equation 4}$$

where σ_{rms} is the root-mean-square. For a function where the mean is zero, the root-mean-square is equal to the standard deviation. Therefore:

$$A = \sqrt{2}\sigma_{n} \qquad\qquad \text{Equation 5}$$

where σ_n is the standard deviation. It has been observed that the vibration were dominated by a single mode and that this modal component was approximately sinusoidal. The peak-to-peak amplitude of vibration $\hat{Y}$ can be estimated as:

$$\hat{Y} = 2A = 2\sqrt{2}\sigma_{n} \qquad\qquad \text{Equation 6}$$

A method to determine the stresses caused by displacements in a beam is to estimate an equivalent load that would produce the same displacements. Having an equivalent load allows for the calculation of reactions and stresses. To determine the equivalent load, the cantilever beam shown in Figure was taken into consideration. If it is assumed that only the first mode shape of the beam is significant, the load p(x, t) can be calculated as follows:

$$p(x, t) = m(x)\, \omega_1^2\, \Phi_1(x)\, q(t) \qquad\qquad \text{Equation 7}$$

where:

  x = distance from fixed end

  t = time

  m(x) = mass per unit length

  ω_1 = first natural frequency in radians per second

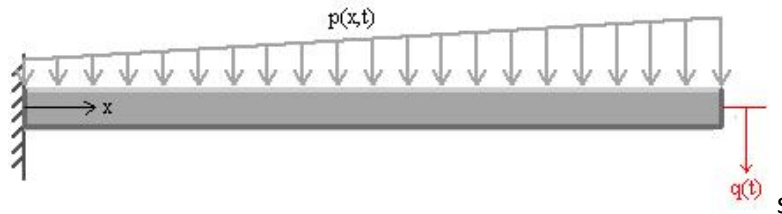 $\phi_1(x) = 1^{st}$ mode shape

  q(t) = tip displacement

Figure 11. Cantilever Beam Subjected to Load p(x,t) and Having Tip Displacement q(t).

Therefore, to determine the equivalent load, the mass per unit length, the first natural frequency, and the first mode shape need to be determined. For the 44-ft mast arm being analyzed here, the vertical fundamental frequency has already been determined on the full-scale prototype as f_o = 0.98 Hz, thus $\omega_1 = 2\,\pi\, f_o = 6.157$ rad/sec.

  Making the following definition:

$$p_o(x) = m(x)\, \omega_1^2\, \phi_1(x) \qquad\qquad \text{Equation 8}$$

  then Equation 7 becomes:
$$p(x, t) = p_o(x)\, q(t) \qquad\qquad \text{Equation 9}$$

To determine the mode shape, a finite element model of the 44-ft mast arm was made using a demo version of the commercial software RISA-3D version 6 by RISA Technologies and is shown in Figure 11. Also shown in Figure 11 is the mass per unit length determined by the following formula:

$$m(x) = (\pi\, \gamma\, /\, 4g)\, \{[OD(x)]^2 - [OD(x) - 2t]^2\} \qquad \text{Equation 10}$$

where:

  x = longitudinal coordinate of the node, zero at the arm-to-post connection

  γ = unit weight of steel = 0.283 lb/in^3

  g = acceleration due to gravity = 386.4 in/sec^2

  OD(x) = outside diameter of mast arm = 11.4 - 0.01188x (for OD and x in inches)

  t = wall thickness of the mast arm = 0.25 in

15

Table 3. Results of Dynamic Analysis

Node	x (in)	m(x) [(lb-sec^2/in)/in]	$\phi_1(x)$	$p_o(x)$ [(lb/in)/in]
1	0	0.0064	0.00	0.0000
2	12	0.0063	0.01	0.0017
3	24	0.0062	0.01	0.0035
4	36	0.0062	0.02	0.0054
5	48	0.0061	0.03	0.0075
6	60	0.0060	0.04	0.0097
7	72	0.0059	0.05	0.0120
8	84	0.0058	0.07	0.0144
9	96	0.0058	0.08	0.0169
10	108	0.0057	0.09	0.0196
11	120	0.0056	0.11	0.0223
12	132	0.0055	0.12	0.0251
13	144	0.0054	0.14	0.0280
14	156	0.0053	0.15	0.0309
15	168	0.0053	0.17	0.0339
16	180	0.0052	0.19	0.0369
17	192	0.0051	0.21	0.0400
18	204	0.0050	0.23	0.0431
19	216	0.0049	0.25	0.0463
20	228	0.0049	0.27	0.0495
21	240	0.0048	0.29	0.0526
22	252	0.0047	0.31	0.0558
23	264	0.0046	0.34	0.0589
24	276	0.0045	0.36	0.0621
25	288	0.0044	0.39	0.0652
26	300	0.0044	0.41	0.0682
27	312	0.0043	0.44	0.0712
28	324	0.0042	0.47	0.0742
29	336	0.0041	0.49	0.0771
30	348	0.0040	0.52	0.0799
31	360	0.0040	0.55	0.0826

Table 3 (continued)

32	372	0.0039	0.58	0.0852
33	384	0.0038	0.61	0.0877
34	396	0.0037	0.64	0.0901
35	408	0.0036	0.67	0.0924
36	420	0.0035	0.70	0.0946
37	432	0.0035	0.74	0.0966
38	444	0.0034	0.77	0.0984
39	456	0.0033	0.80	0.1001
40	468	0.0032	0.83	0.1016
41	480	0.0031	0.87	0.1029
42	492	0.0031	0.90	0.1041
43	504	0.0030	0.93	0.1050
44	516	0.0029	0.97	0.1058
45	528	0.0028	1.00	0.1064

Also shown in Table 3 is the product $p_o(x)$, calculated using Equation 8.

$$p_o(x) = -9E\text{-}10x^3 + 6E\text{-}07x^2 + 0.0001x + 0.0002$$
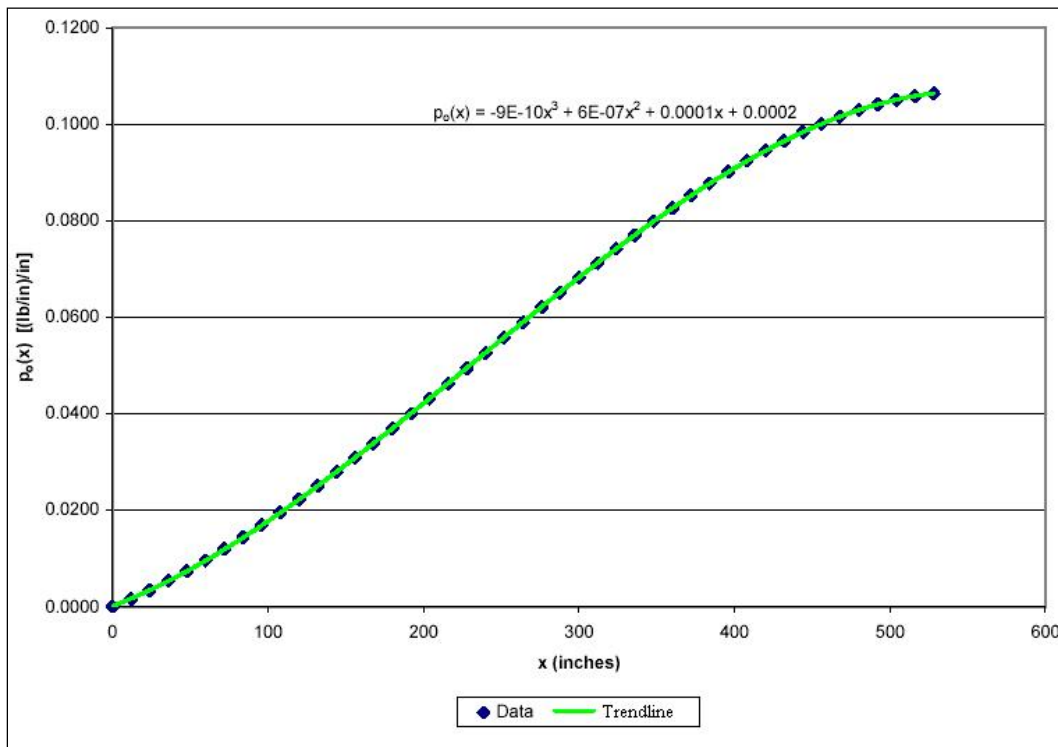
Figure 12. x vs. $p_o(x)$

Using Microsoft Excel, a plot of x vs. $p_o(x)$ was obtained, as well as a cubic equation of a trendline that adjusted very well to the data, as shown in Figure 12. This equation will be used in further calculations.

Figure 13 shows the loads acting on the mast arm. In this figure, $P_1(t)$, $P_2(t)$, and $P_3(t)$ represent the dynamic loads caused on the arm by the 3 signals while V and M are the shear and moment reactions, respectively, at the base of the arm. To calculate the loads due to the signals, the following formula is used:

$$P_i(t) = m_i \omega_1^2 \phi_1(x_i) q(t) \qquad\qquad \text{Equation 11}$$

where m_i is the mass of the signal light and is $\phi_1(x_i)$ is the value of the mode shape at the x_i location.
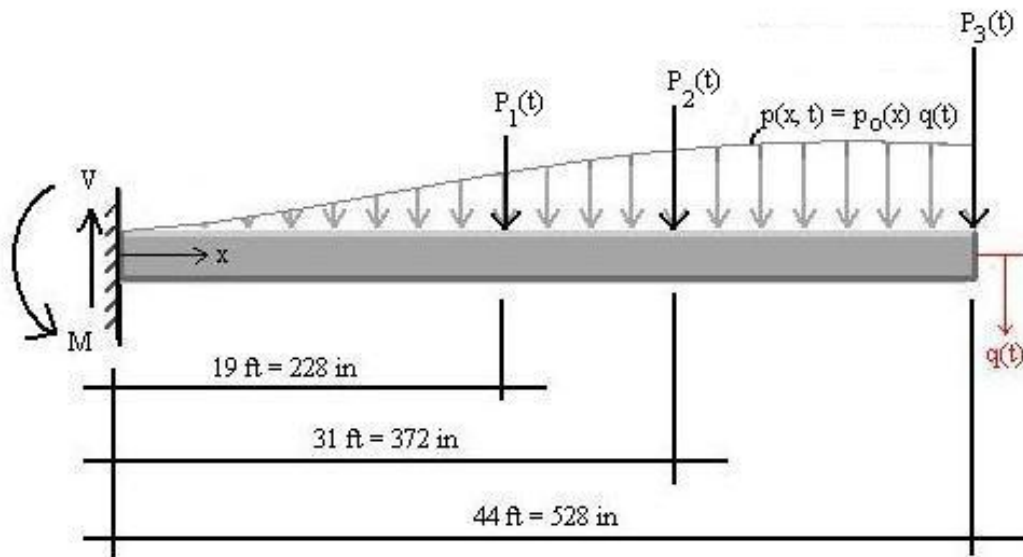
Figure 13. Loads Acting on Mast Arm

Adding moments about the fixed support:

$$M = 228 \cdot P_1(t) + 372 \cdot P_2(t) + 528 \cdot P_3(t) + \int_0^{528} x\, p(x, t)dx \qquad \text{Equation 12}$$

Substituting Equation 9, Equation 11 and the $p_o(x)$ equation presented in Figure 12:

$$M = 13{,}820\ q(t) \qquad\qquad \text{Equation 13}$$

where q(t) must be entered in inches and M will be given in pounds-inches.

To determine the maximum bending stress σ_{max} of the mast arm at the arm-to-post connection, the basic flexure formula is used:

18

$$\sigma_{max} = \frac{Mc}{I}$$
                                                                    Equation 14

where I is the moment of inertia of the cross-section and c is the perpendicular distance from the neutral axis of the cross-section to the farthest point away from the axis. Using the dimensions of the mast arm at the arm-to-post connection as given by and substituting Equation 13:

$\sigma_{max} = 578.55\ q(t)$ Equation 15

where q(t) must be entered in inches and σ_{max} will be given in pounds per square inch.

Substituting values of displacement in Equation 15 will not give the total stress on the structure, but it will give the change of stress in the structure. By substituting values of peak-to-peak vibration amplitudes $\hat{Y}$, the equation will give the stress ranges S:

$S = 578.55\ \hat{Y}$ Equation 16

where $\hat{Y}$ must be entered in inches and S will be given in pounds per square inch. The stress range S is the magnitude of the stress peak-to-peak amplitude.

The constant-amplitude fatigue level (CAFL) is the stress range below which the fatigue life appears infinite, i.e. there is no fatigue damage when the stress ranges are below the CAFL. Using the AASHTO Specifications (2001), the mast-arm connection is identified as having a stress category E'. With this information, the CAFL can be determined from the AASHTO's *Standard specifications for highway bridges* (1996). Knowing that CAFL = 2.6 ksi, the minimum peak-to-peak vertical vibration amplitude that causes significant fatigue loading in the 44-ft mast arm can be calculated from Equation 16 as follows:

$2600 = 578.55\ \hat{Y}$ Equation 17

$\hat{Y} = 4.5$ inches   Equation 18

Then, using Equation 6, the minimum standard deviation of the vertical vibration at which significant fatigue loading occurs can be estimated:

$4.5 = 2\sqrt{2}\sigma_n$ Equation 19

$\sigma_n = 1.6$ inches   Equation 20

Therefore, for the 44-ft mast arm analyzed in this research, it is estimated that significant fatigue loading occurs when the standard deviation of the vertical displacement (Y) is equal to or larger than 1.6 inches, or when the peak-to-peak amplitude of the vertical displacement is equal to or larger than 5.66 inches.

Performing the same analysis for the 60-ft arm, the following equation is obtained:

$S = 315.23\ \hat{Y}$ Equation 21

The 60-ft arm also has a stress category E' connection to its mast, therefore its CAFL is 2.6 ksi. The minimum peak-to-peak vertical vibration amplitude that causes significant fatigue loading in the 60-ft mast arm can be calculated from Equation 16 as follows:

$$2600 = 315.23 \ \hat{Y} \qquad\qquad \text{Equation 22}$$

$$\hat{Y} = 8.25 \text{ inches} \qquad\qquad \text{Equation 23}$$

Then, using Equation 6, the minimum standard deviation of the vertical vibration at which significant fatigue loading occurs can be estimated:

$$8.25 = 2\sqrt{2}\sigma_n \qquad\qquad \text{Equation 24}$$

$$\sigma_n = 2.9 \text{ inches} \qquad\qquad \text{Equation 25}$$

Therefore, for the 60-ft mast arm analyzed in this research, it is estimated that significant fatigue loading occurs when the standard deviation of the vertical displacement (Y) is equal to or larger than 2.9 inches.

Results

In this section two sets of results are discussed: (1) the preliminary data obtained on March 25, 2005 for TS2 with the arm pointing east and the signals with backplates and (2) the data obtained under Mode 1100.

March 29, 2005

On March 29, 2005, with TS2 (having a 44-ft arm) being recently operational and pointing east, the instrumentation recorded vertical vibrations of the arm tip with peak to peak oscillations as large as 11 inches. Presented in Figure 14 are 10 hours of the recorded data. In this case, the wind speed component perpendicular to the mast arm approached the structure from the back of the traffic signals while the component parallel to the mast arm moved from the mast to the tip of the arm.
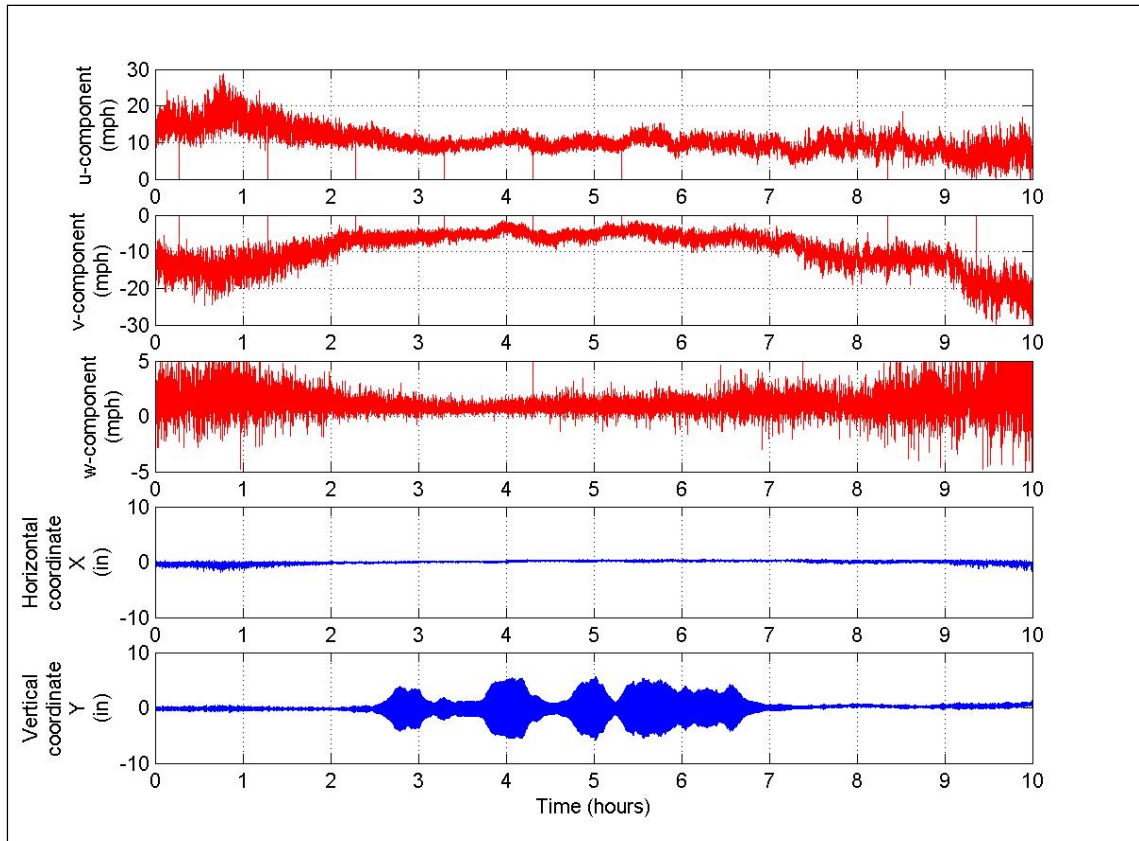
Figure 14. Wind and Displacement Data Collected on March 29, 2005

The following observations were made:

1. Horizontal vibrations had large amplitudes when the wind was more turbulent.

2. Vertical vibrations had larger amplitudes when the perpendicular wind speed averaged about 10 mph.

3. Vertical vibrations reached much higher amplitudes than horizontal vibrations.

4. When the vertical vibrations were larger, the horizontal vibrations were smaller and vice versa.

5. The 11-in peak-to-peak oscillations would produce stress ranges of 6.36 ksi in the mast arm at the end connected to the pole.

After evaluating sample lengths of between 30 and 300 seconds, the 100-cycle sample was selected for subsequent analyses. Knowing that the fundamental frequency of the structure is close to 1 Hz, the data presented in Figure 14 was divided into smaller segments of 100 seconds. For each segment the mean and the standard deviation of the total wind speed and the angle of attack were calculated, along with the standard deviation of the horizontal and the vertical displacements. These values were used to produce the plots presented in Figure 15 to Figure 22.

21

These graphs are done to establish a relation between commonly measured wind data (speed, turbulence intensity and direction) and displacement in the tip of the arm. Mean values of the displacements would be zero, therefore they are not useful. The standard deviation of the displacement is used instead, because this provides an average of how much the arm extended from its "zero" position.

Figure 15 shows that low-amplitude horizontal vibrations occurred when the mean wind speed was about 10 mph and that vibrations increased as the total wind speed increased. In Figure 16 it can be seen that high-amplitude vertical vibrations were observed when the total wind speed was between 10 and 12 mph. From Figure 17 no clear relationship can be established between the horizontal vibrations and the turbulence intensity. Likewise, no relationship can be established clearly between the vertical vibrations and the turbulence intensity by observing Figure 18.

Figure 19 demonstrates that there was more scatter in the horizontal vibrations when the angle of attack was over 130°. Figure 20 shows that larger vibrations occurred when the angle of attack was below 130°. In Figure 21 it can be seen that larger horizontal vibrations occurred when there was higher variability in the angle of attack. To the contrary, Figure 22 shows that higher vertical vibrations occurred when the angle of attack was less variable.
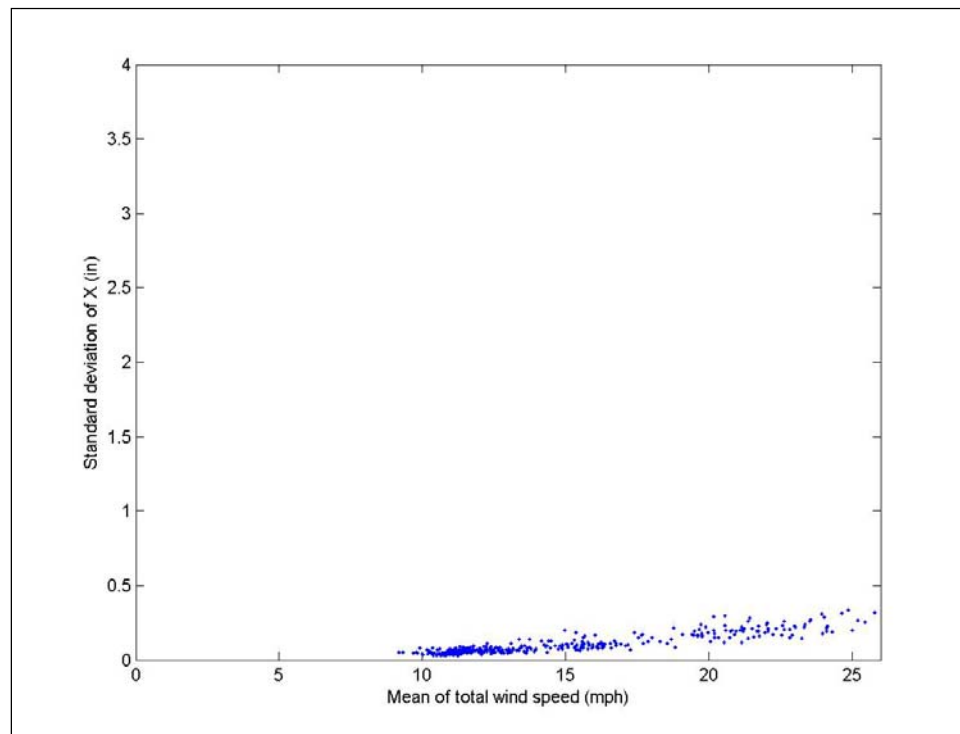
Figure 15. Effect of Wind Speed on Horizontal Vibrations of Arm
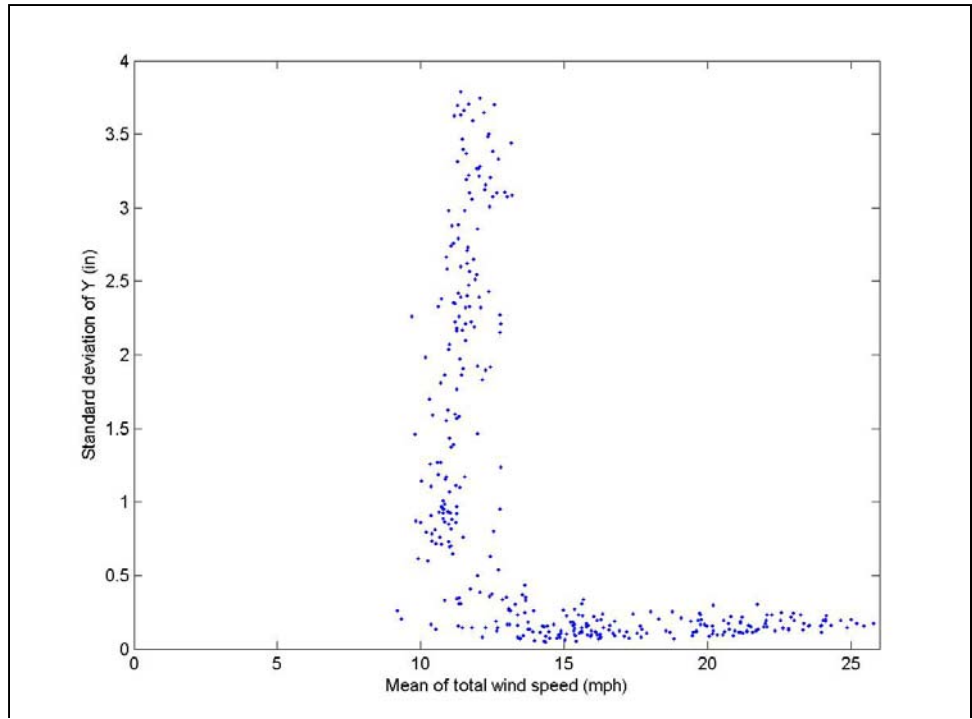
Figure 16. Effect of Total Wind Speed on Vertical Vibrations of Arm
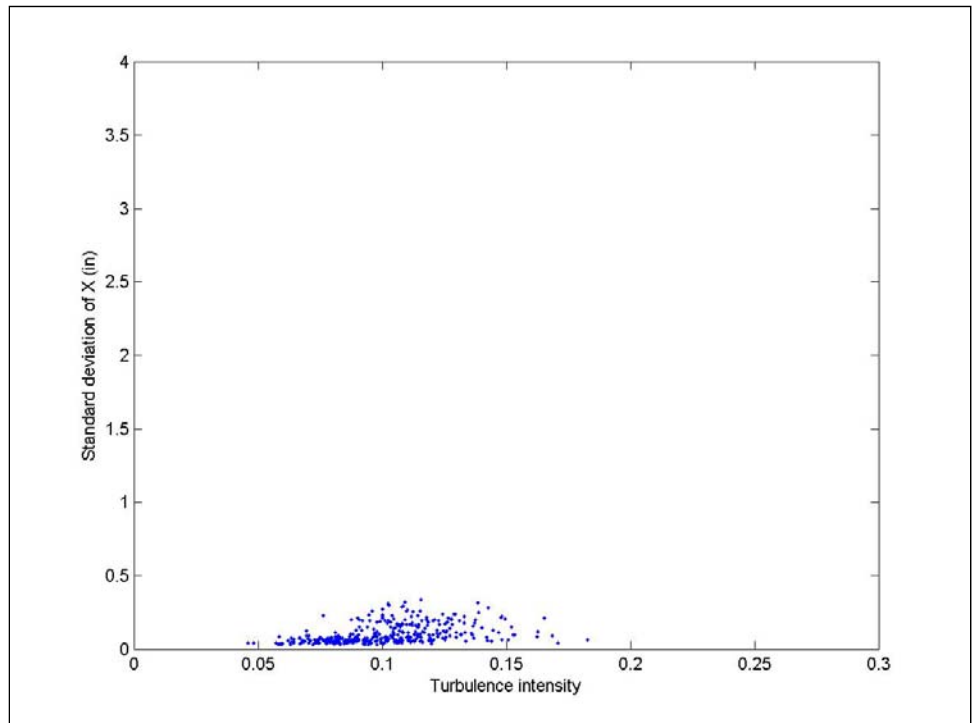
Figure 17. Effect of Turbulence on Horizontal Vibrations of Arm

0-4586-3
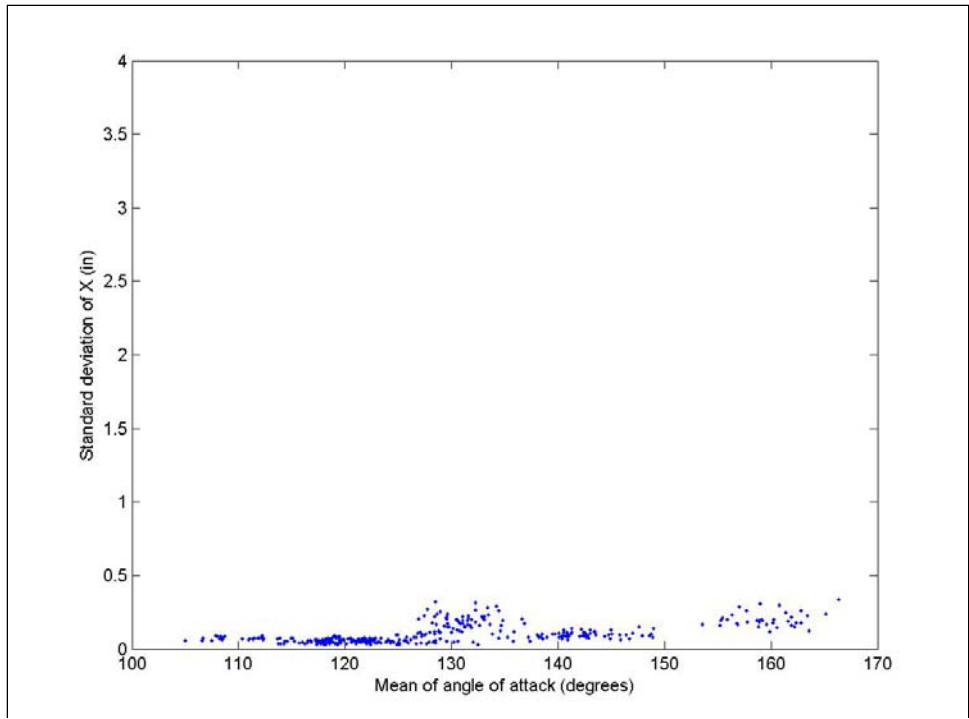
Figure 18. Effect of Turbulence on Vertical Vibrations of the Arm
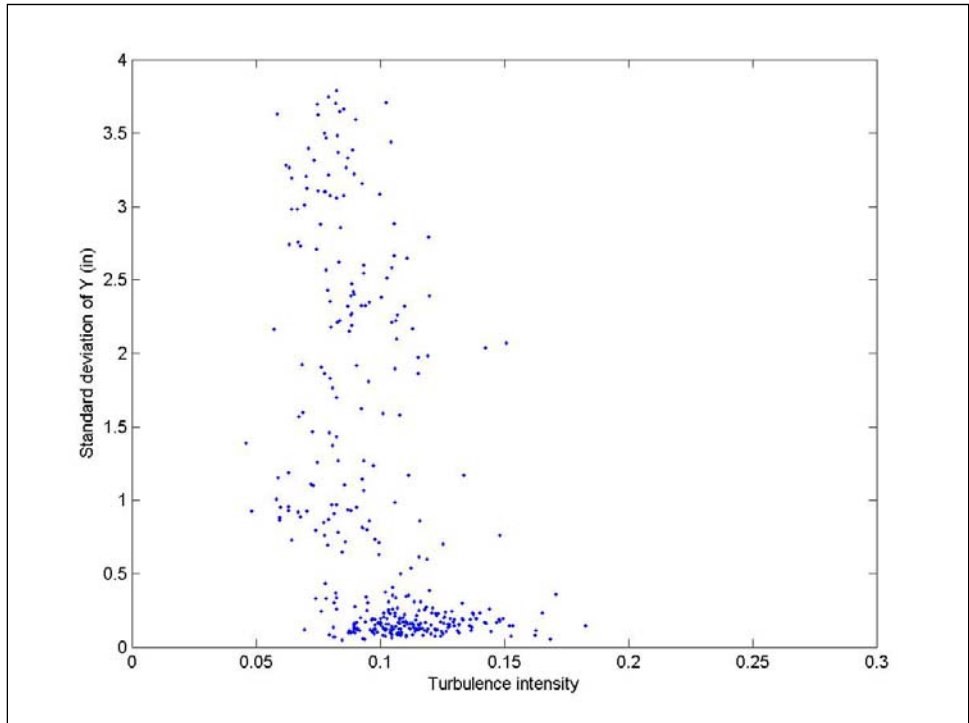
Figure 19. Effect of Wind Angle of Attack on Horizontal Vibrations

24
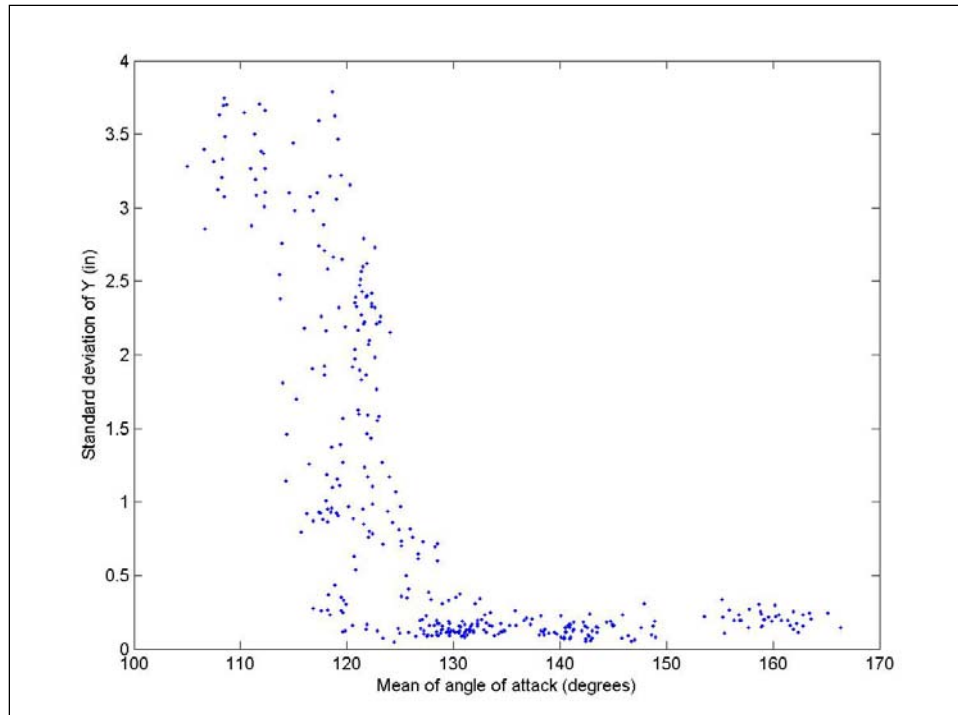
Figure 20. Effect of Wind Angle of Attack on Vertical Vibrations
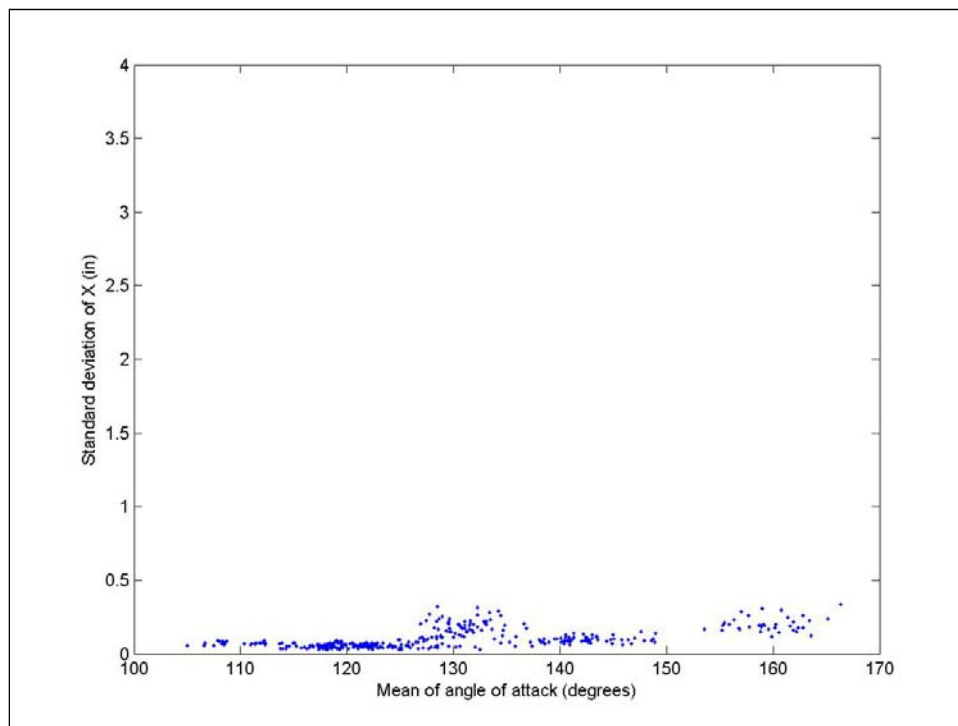
Figure 21. Effect of Variations in Angle of Attack on Horizontal Vibrations
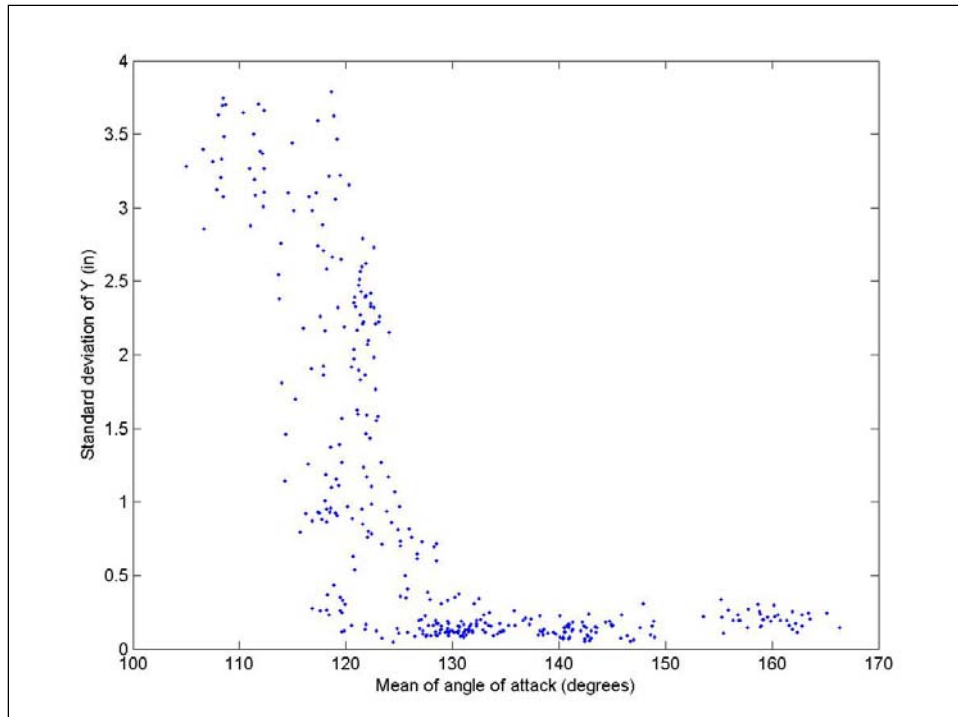
Figure 22. Effect of Variations in Angle of Attack on Vertical Vibrations

Figure 15 through Figure 22 were plotted using data segments of 100 seconds. It should be noted that data was also analyzed using longer and shorter segments and the same trends were observed. An example of this is shown in Figure 23, in which the effect of the total wind speed on vertical vibrations is plotted using both 100- and 300-second segments. In both cases it can be seen that high-amplitude vertical vibrations are observed when the total wind speed is between 10 and 12 mph.
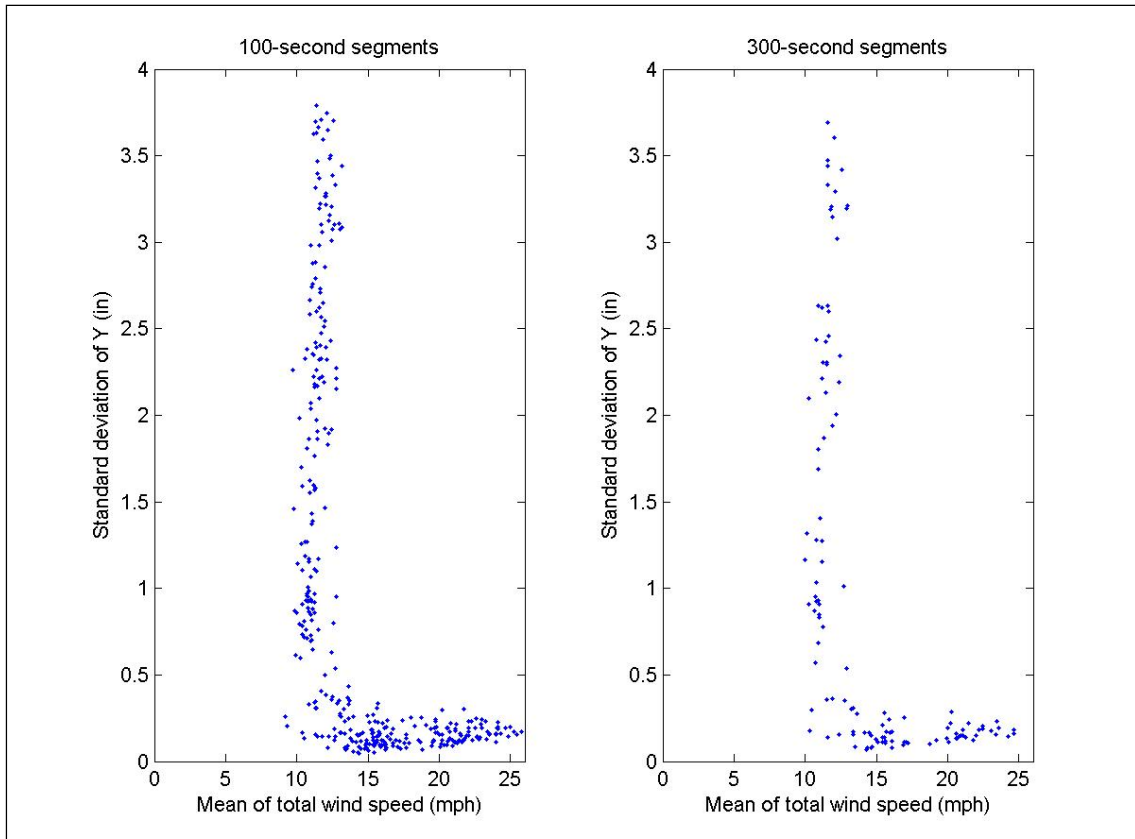
Figure 23. Comparison of Data Analysis using Segments of 100 and 300 Seconds

The Strouhal number when the wind was approximately perpendicular to the backplate vibrating at 0.98 Hz and using a cross-wind body width (*B*) of a traffic signal head with backplate is:

$$St = \frac{fB}{U} = \frac{(0.98\ \text{Hz})\,(23\ \text{in})}{11\ \text{mph}} = \frac{(0.98\ \text{Hz})\,(1.92\ \text{ft})}{16\ \text{ft/sec}} = 0.12$$

This Strouhal number is close to the published value of 0.15 for a flat plate perpendicular to the flow (Blevins 1977; Hirsch and Bachmann 1995) and the response exhibits the classic lock-in phenomena for vortex shedding.

Mode 1100 (Mast pointing North, signals with backplates)

From April 2005 to March 2006, data was collected under Mode 1100. During this period, over 5,000 hours of data were collected. Out of those, 310 hours were identified as having at least one of the X and Y displacements having a standard deviation for the hour equal or greater than 0.5 inches.

The 310 hours were further analyzed by dividing them into 2-minute segments, calculating summary statistics (mean and standard deviations) for different measured parameters and plotting graphs. Some of the graphs are presented and discussed here. To see all the plotted graphs, refer to Appendix B.

Figures 24 and 25 show the effect the wind speed component perpendicular to the arm has on the vertical vibrations of the TS1 and TS2, respectively. A positive perpendicular speed means that it approaches the mast arm from behind the signals. In the case of the TS1, there seems to be higher vibrations at -10 and +7 mph, but very few times the standard deviation of Y went over 2.9 inches (the standard deviation that when exceeded produces fatigue damage to TS1). The few times that it did, it was mostly in the speed range of 0 to+10 mph. For TS2, there were more cases of the standard deviation of Y exceeding 1.6 inches, and most of them were also in the 0 to +10 mph range, with three cases in the -5 to 0 mph range.
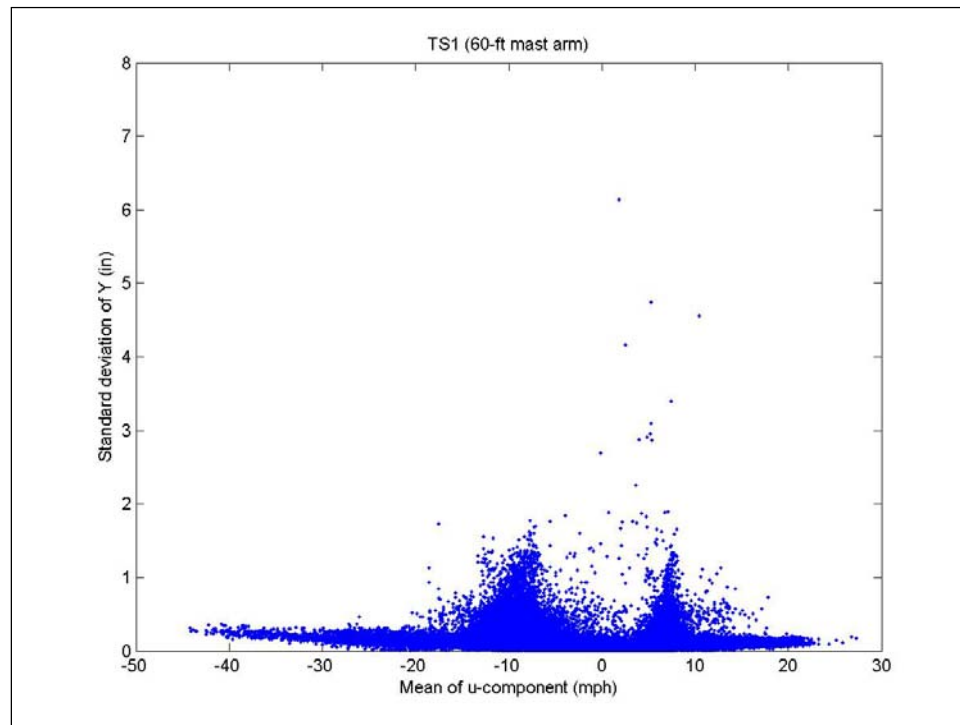
Figure 24. Effect of Perpendicular Wind Speed Component on Vibrations of TS1
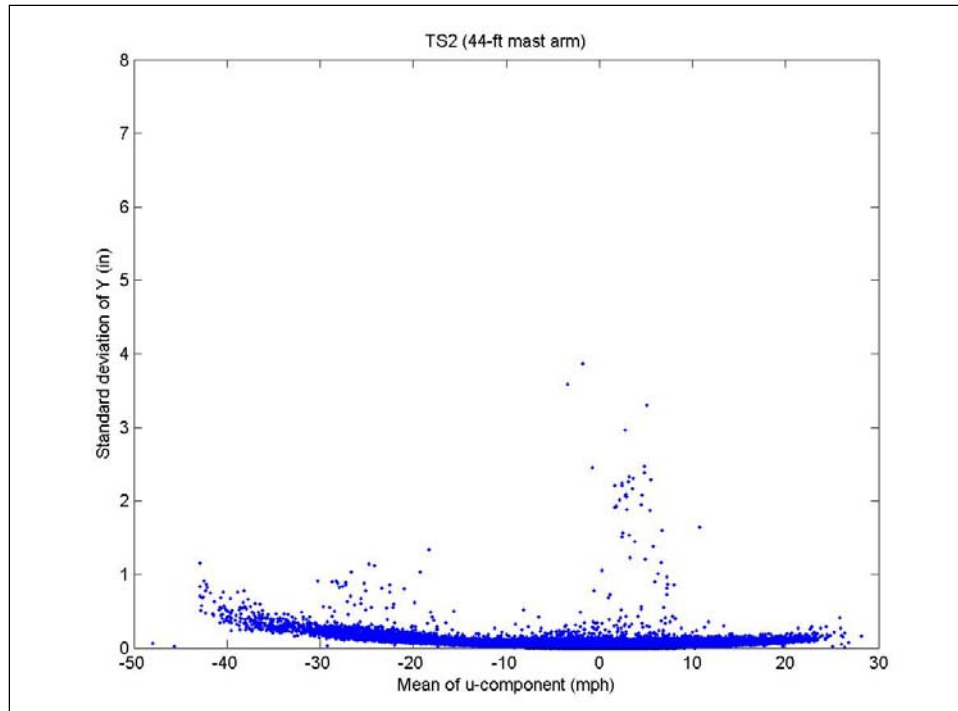
Figure 25. Effect of Perpendicular Wind Speed Component on

Vertical Vibrations of TS2

Figures 26 and 27 on the following page show the effect of mean wind speed (the vectorial sum of the perpendicular and parallel components) on the vertical vibrations of the mast arm of TS1 and TS2, respectively. Notice that in both cases, the standard deviation of Y never exceeds the significant fatigue loading limit (2.9" and 1.6", respectively) when the mean speed is over 25 mph. In the case of TS2, there are barely any vibrations when the mean wind speed is over 60 mph.

29
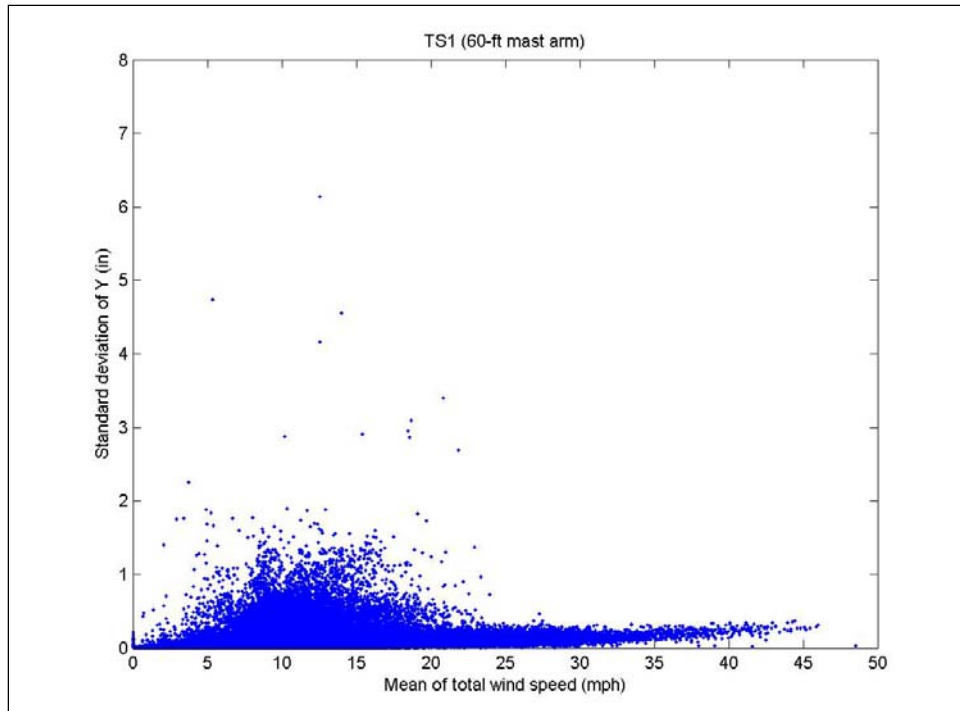
Figure 26. Effect of Mean Wind Speed on Vertical Vibrations of TS1
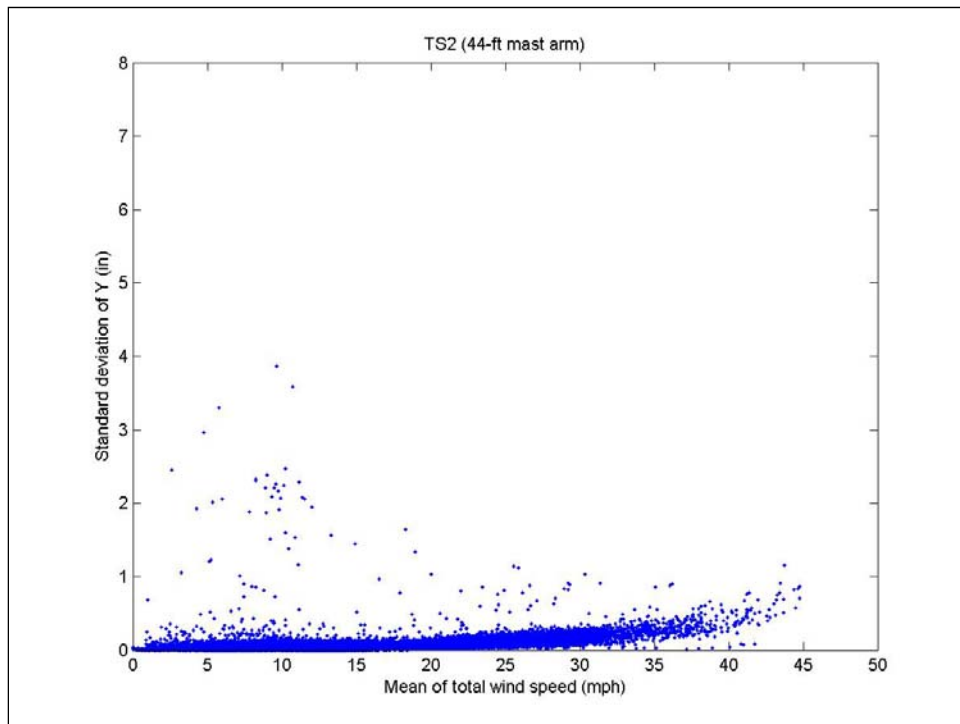
Figure 27. Effect of Mean Wind Speed on Vertical Vibrations of TS2

Figures 28 and 29 show the effect the wind direction has on the vertical vibrations of the arms of TS1 and TS2, respectively (the sign convention of the angle of attack is given in Figure 7.) For the case of TS1, there are a concentration of cases at around 60 and 300 degrees, but again very few cases exceeded a standard deviation of Y of 1.6 inches. For both TS1 and TS2, higher vibrations (standard deviation of Y exceeding the limits of 2.9" and 1.6", respectively) occur between 0 and 180 degrees, which corresponds to when there is a wind component blowing from the back of the signals.
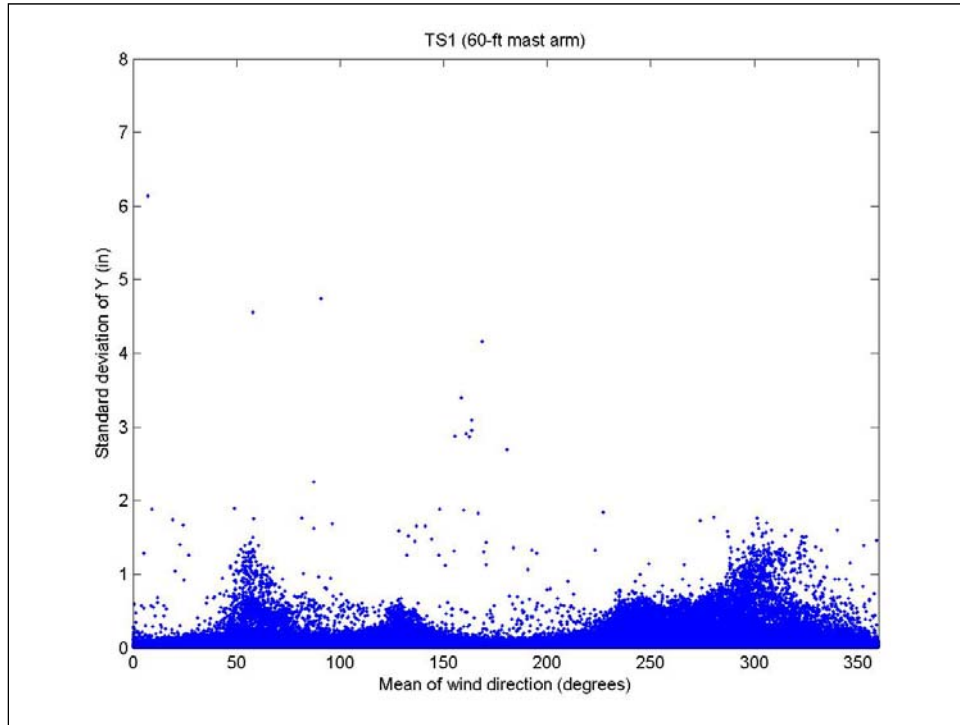
Figure 28. Effect of Angle of Attack on Vertical Vibrations of TS1

0-4586-3
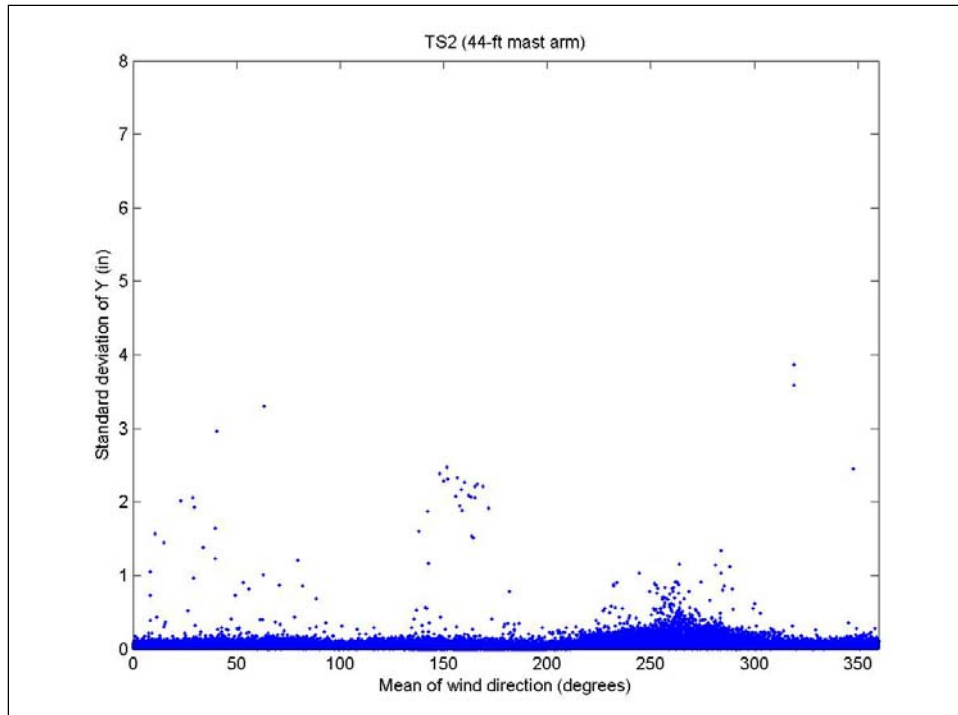
Figure 29. Effect of Angle of Attack on Vertical Vibrations of TS2

Conclusions

It has been observed throughout this experiment that large amplitude vertical vibrations of mast arms with signals with backplates occur for the most part at low wind speed ranges, and as the wind speed increases the amplitude of the vertical vibrations decreases. Having large vibrations at a certain wind speed range reflects the typical behavior of vibrations induced by vortex shedding. This contradicts the theory that vortex shedding does not cause large-enough vibrations of mast/arms that could lead to fatigue failure. Large vibrations are generally attributed to galloping (AASHTO; Cook et al; Dexter & Ricker, Kaczinski et al; Pulipaka et al) where vibration amplitude increases with wind speed. Such galloping was not observed in this study.

It seems that the higher amplitude vertical oscillations have a higher probability of occurring when the wind speed is steady (i.e. has low turbulence) between 5 to 10 mph. It also appears that oscillations are more likely to occur when the wind approaches the mast arm from the back of the signal.

Very few cases of large vibrations were observed under Mode 1100, possibly because wind conditions were less than ideal. This is a typical difficulty of conducting full-scale experiments. It could be advantageous to include wind tunnel experiments, where the wind conditions are more easily controlled.

References

American Association of State Highway and Transportation Officials (AASHTO), *Standard specifications for highway bridges*. 16th ed. Washington, DC, 1996

American Association of State Highway and Transportation Officials (AASHTO), *Standard and Specifications for Structural Supports for Highway Signs, Luminaires, and Traffic Signals*. 4th ed. Washington, DC, 2001

Blevins, Robert D. 1977. *Flow-induced vibration*. New York: Van Nostrand Reinhold Company.

Chen, Genda, Jingning Wu, Jiaqing Yu, Lokeswarappa R. Dharani, and Michael Barker. 2001. Fatigue assessment of traffic signal mast arms based on field test data under natural wind gusts. *Transportation Research Record*, n. 1770: 188-94.

Cook, R. A., D. Bloomquist, D. S. Richard, and M. A. Kalajian. 2001. Damping of cantilevered traffic signal structures. *Journal of Structural Engineering* 127, n. 12: 1476-83.

Dexter, R. J., and M. J. Ricker. 2002. *National Cooperative Highway Research Program Report 469: Fatigue-resistant design of cantilevered signal, sign, and light supports.* Washington, DC: National Cooperative Highway Research Program.

Gray, B., P. Wang, H. R. Hamilton, and J. A. Puckett. 1999. Traffic signal structure research – Univ. of Wyoming. In *Structural Engineering in the 21st Century: Proceedings of the 1999 Structures Congress held in New Orleans, Louisiana, April 18-19, 1999*, edited by R. Avent and M. Alawady, 1107-10. Reston, VA: American Society of Civil Engineers.

G Systems, Texas Tech University Wind Science and Engineering (WISE) Version 2.0; Structural Performance3 DAQ User Manual, Plano, Texas, January 20, 2005

Hamilton III, H. R., G. S. Riggs, and J. A. Puckett. 2000. Increased damping in cantilevered traffic signal structures. *Journal of Structural Engineering* 126, n. 4: 530-7.

Hartnagel, Bryan A., and Michael G. Barker. 1999. Strain measurements of traffic signal mast arms. In *Structural Engineering in the 21st Century: Proceedings of the 1999 Structures Congress held in New Orleans, Louisiana, April 18-19, 1999*, edited by R. Avent and M. Alawady, 1111-4. Reston, VA: American Society of Civil Engineers.

Hirsch, Gerhard H., and Hugo Bachmann. 1995. Dynamic effects from wind. Appendix H of *Vibration problems in structures: Practical guidelines*, by Hugo Bachman et al. Basel, Switzerland: Birkhäuser.

Kaczinski, M. R., R. J. Dexter, and J. P. Van Dien. 1998. *National Cooperative Highway Research Program Report 412: Fatigue-resistant design of cantilevered signal, sign, and light supports.* Washington, DC: National Academy Press.

Paz, Mario. 2002. *Structural dynamics: Theory and computation.* 4th ed. Boston: Kluwer Academic Publishers.

Pulipaka, Narendra. 1995. Wind-induced vibrations of cantilevered traffic signal structures. PhD dissertation, Texas Tech University.

Pulipaka, Narendra, Partha P. Sarkar, and James R. McDonald. 1998. On galloping vibration of traffic signal structures. *Journal of Wind Engineering and Industrial Aerodynamics* 77 & 78 (Sep-Dec): 327-36.

Appendix A

Foundation with Rotatable Plate

0-4586-3
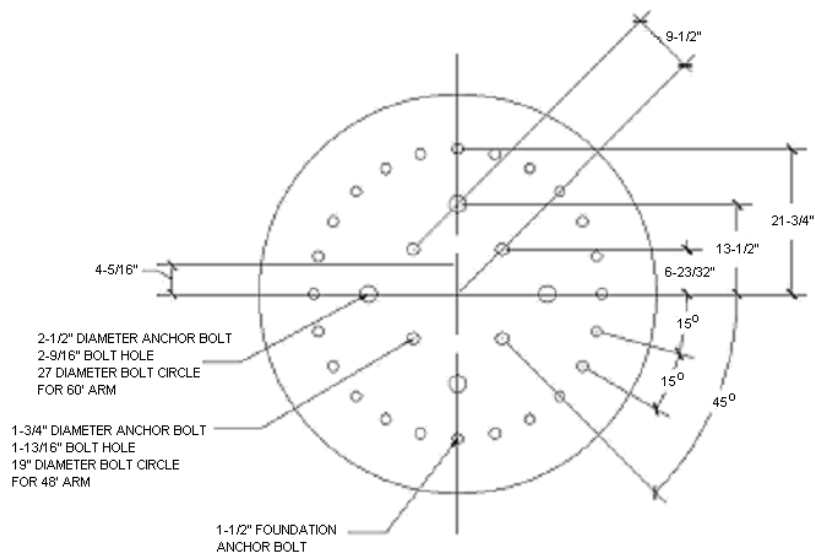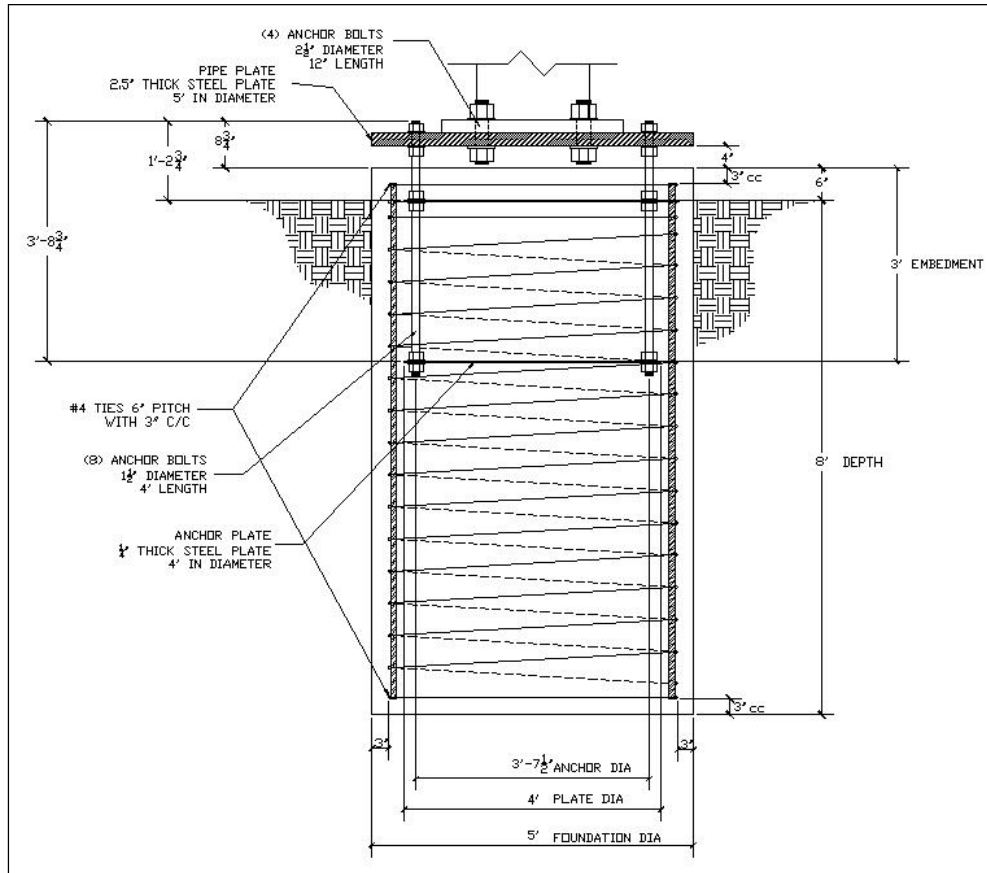
Appendix B – Results for Mode 1100

In this section all the figures obtained by analyzing the data collected under Mode 1100 (arms pointing north, signals with backplates) are shown. A dot on a given plot represents two minutes of data. The sign convention of the angle of attack and of the wind speed components u and v is shown below. The w-component is positive in the upward direction. X and Y refer to out-of-plane (or horizontal) and in-plane (or vertical) displacements of the tip of the arm, respectively.
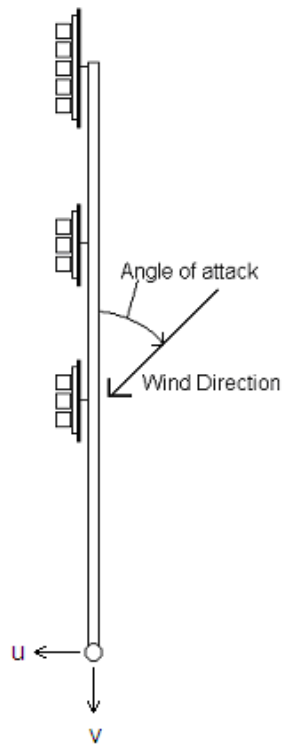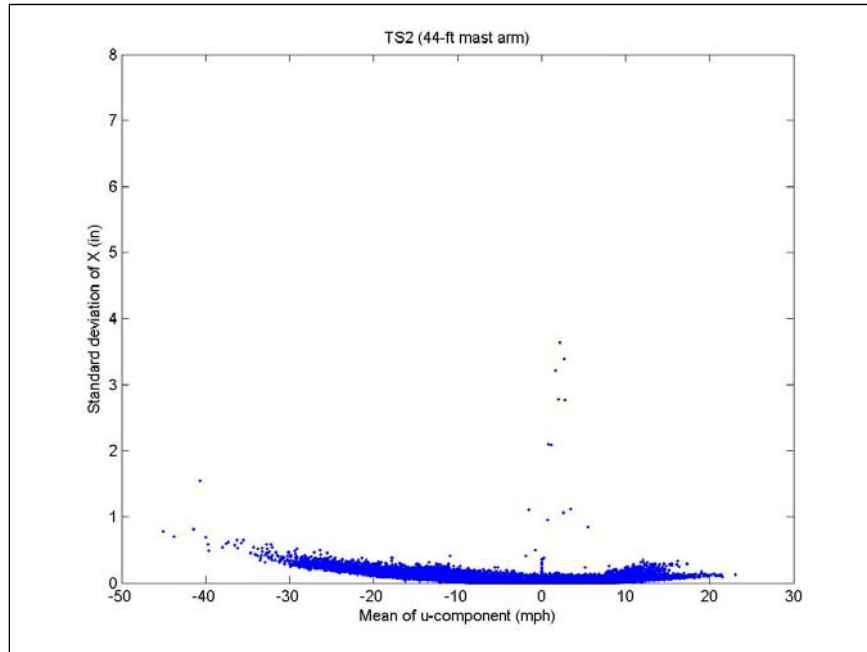

TS1 (60-ft mast arm)
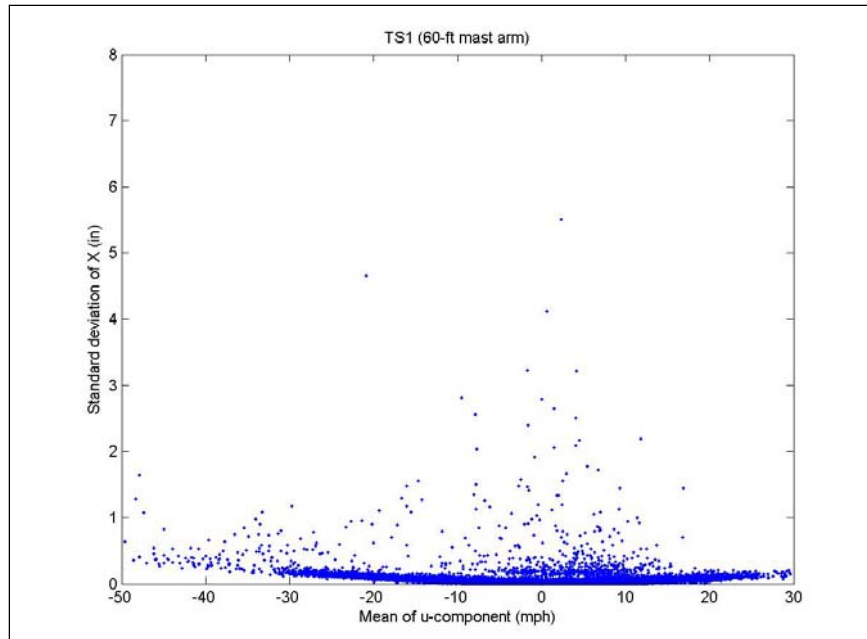
Figure B.1. Effect of u-component on horizontal vibrations of TS1 without backplates
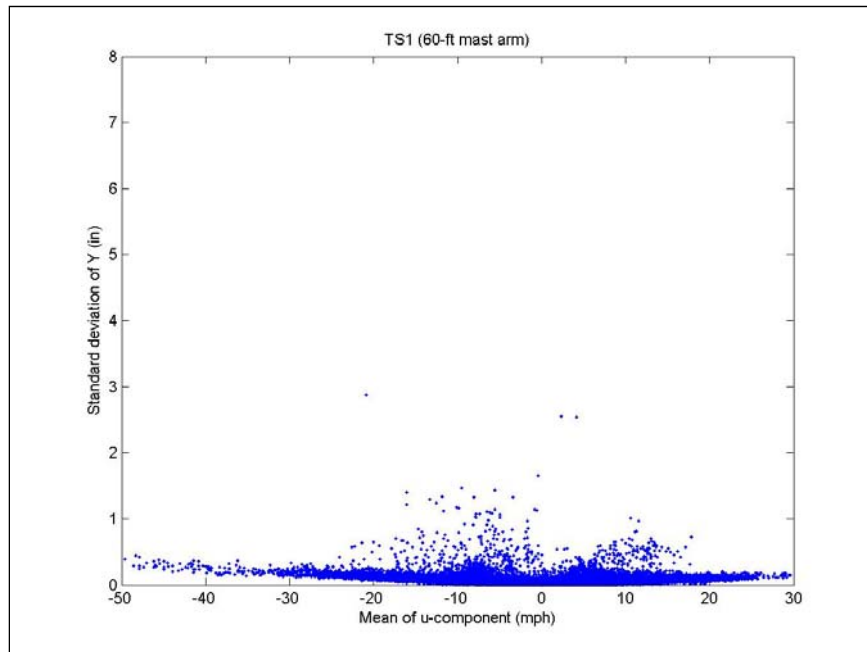
Figure B.2. Effect of u-component on vertical vibrations of TS1 without backplates

0-4586-3
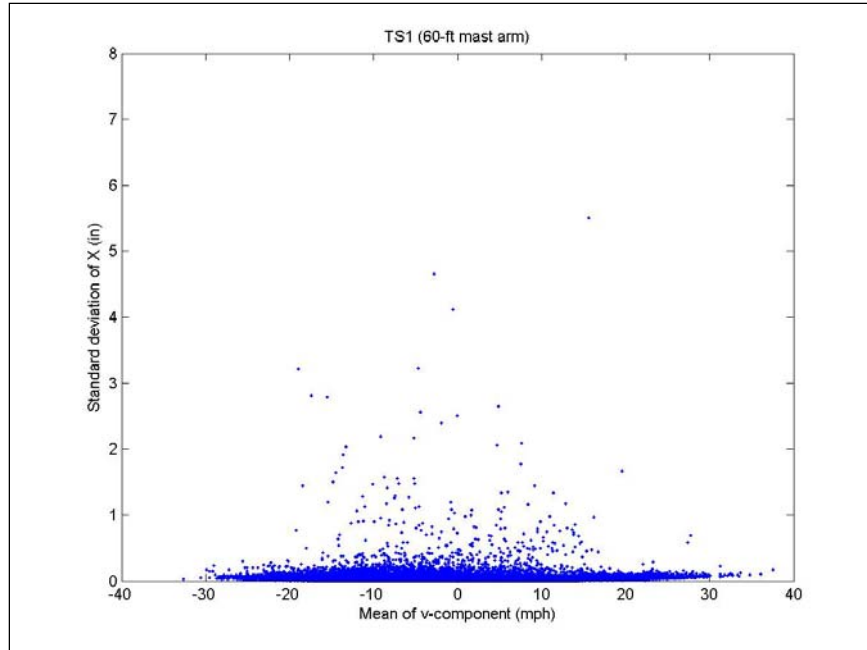
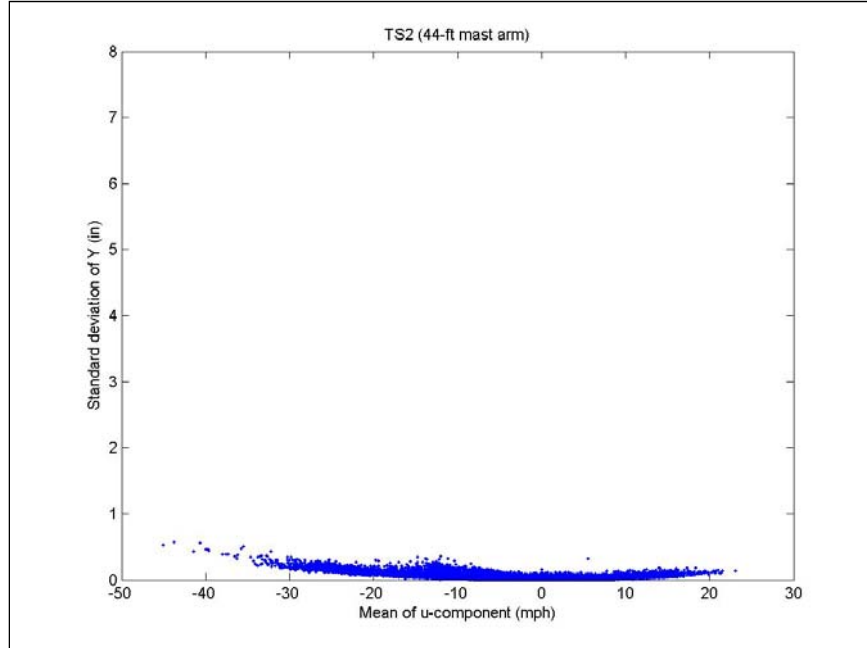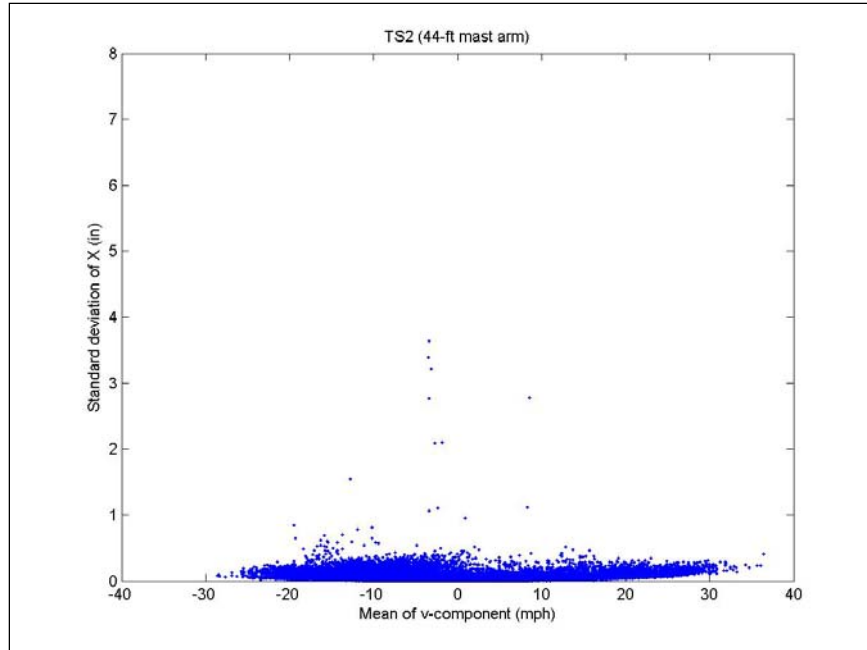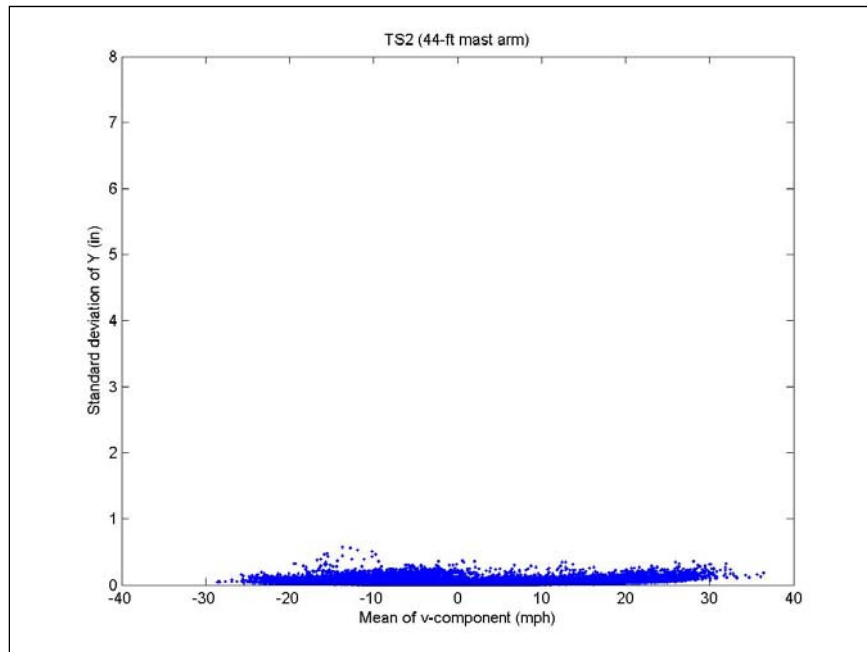Figure B.3. Effect of v-component on horizontal vibrations of TS1 without backplates
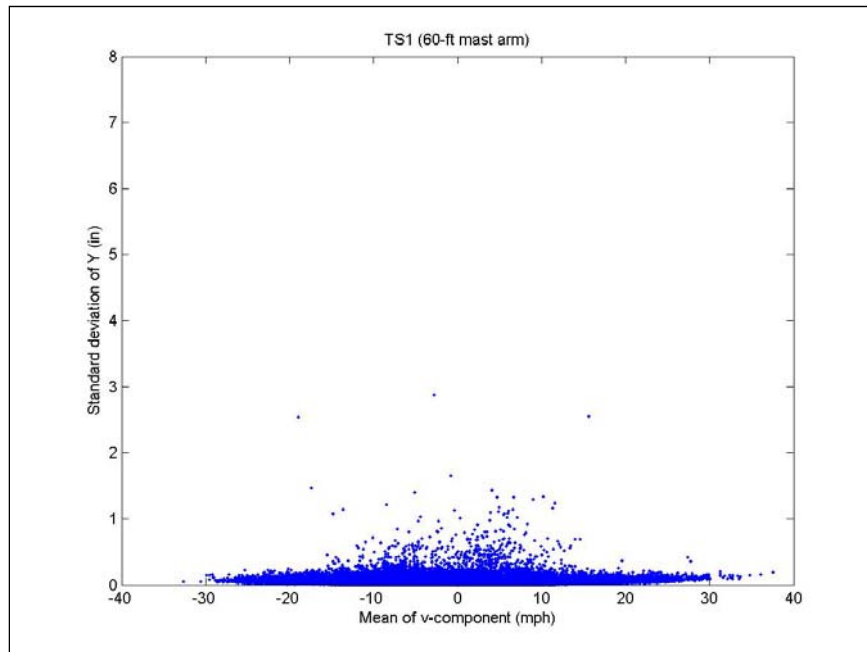
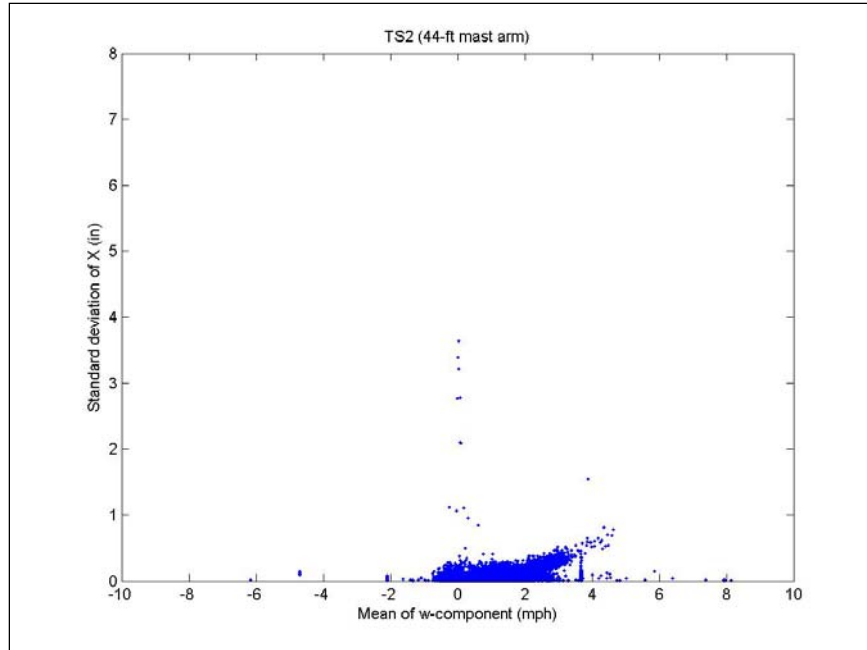Figure B.4. Effect of v-component on vertical vibrations of TS2 without backplates
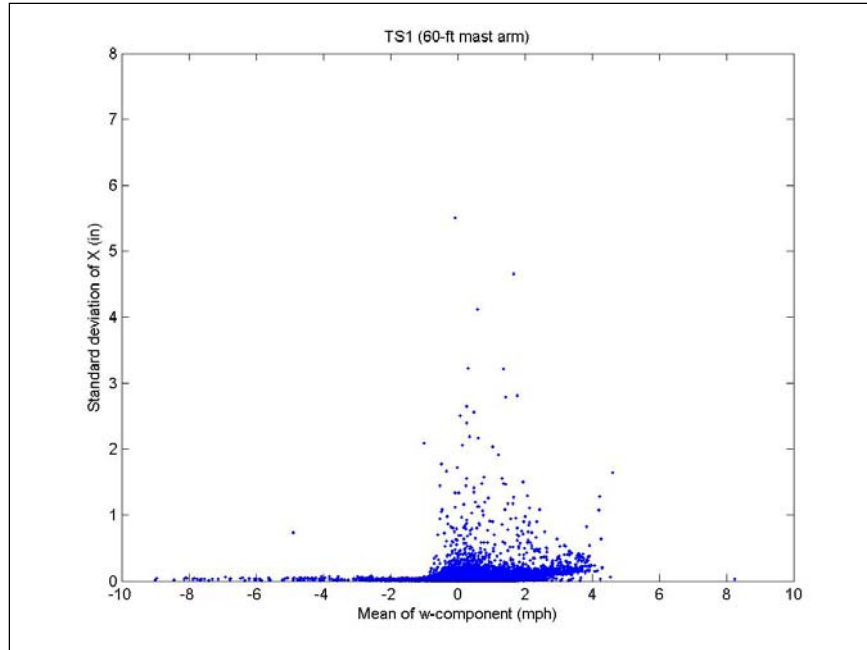
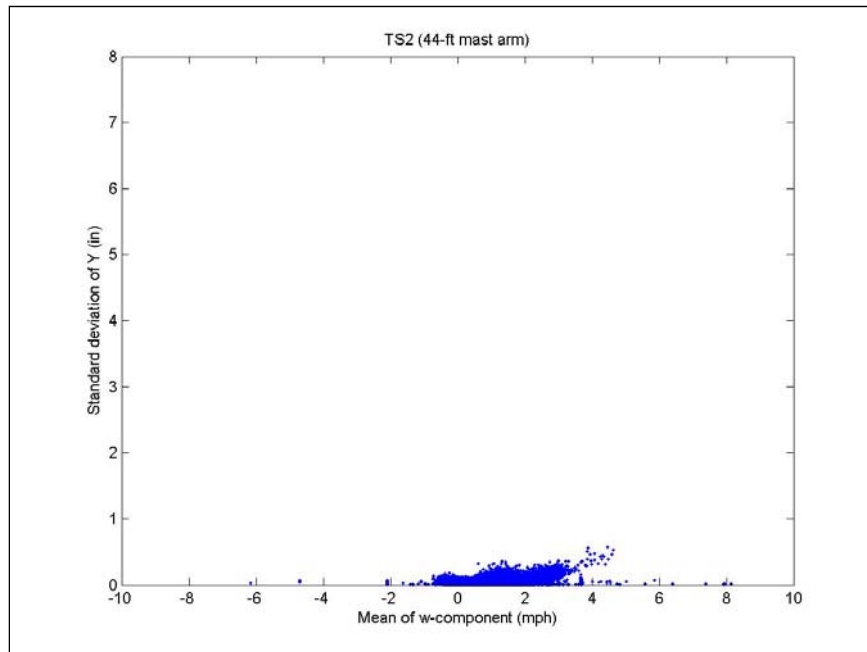Figure B.5. Effect of w-component on horizontal vibrations of TS1 without backplates
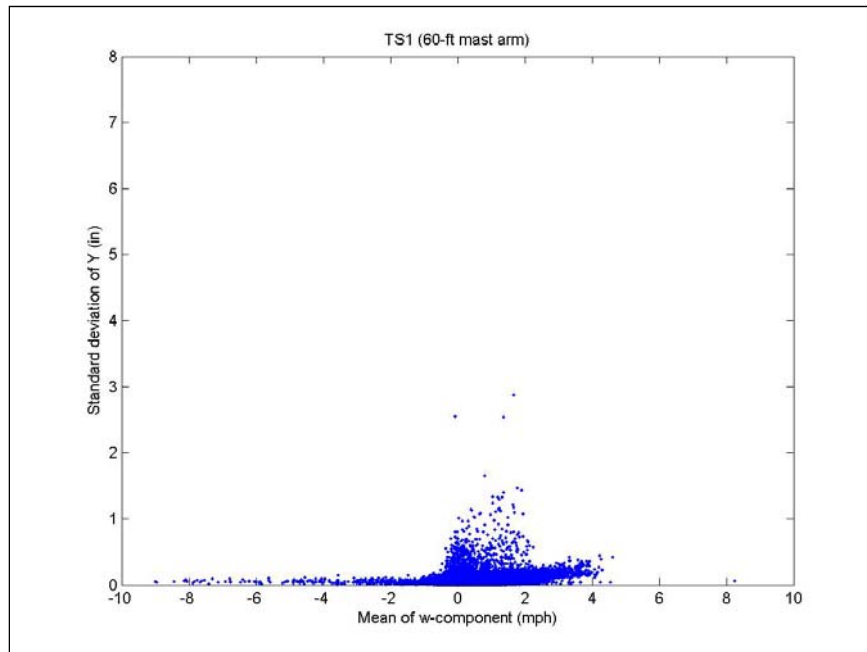
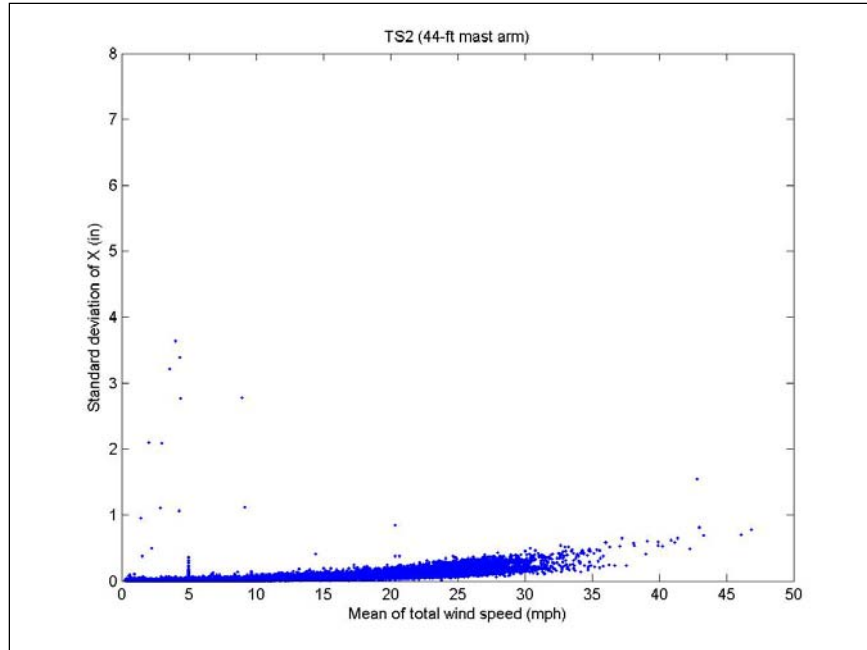Figure B.6. Effect of w-component on vertical vibrations of TS1 without backplates

0-4586-3
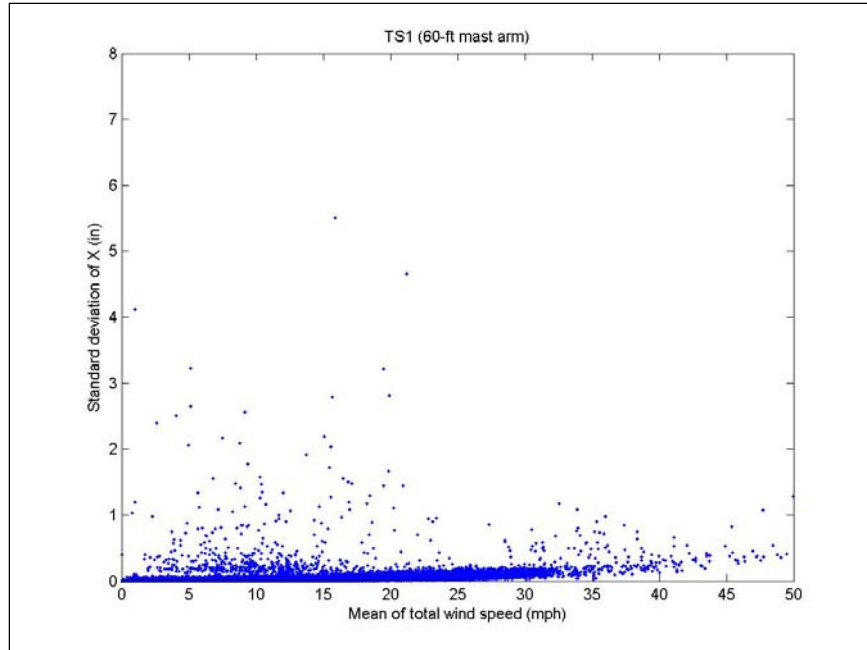
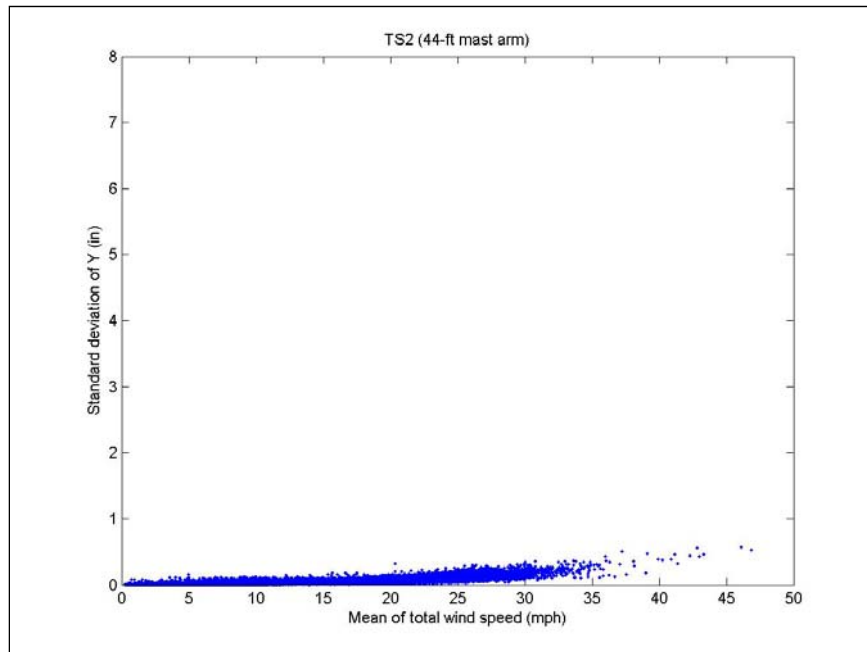Figure B.7. Effect of total wind speed on horizontal vibrations of TS1 without backplates
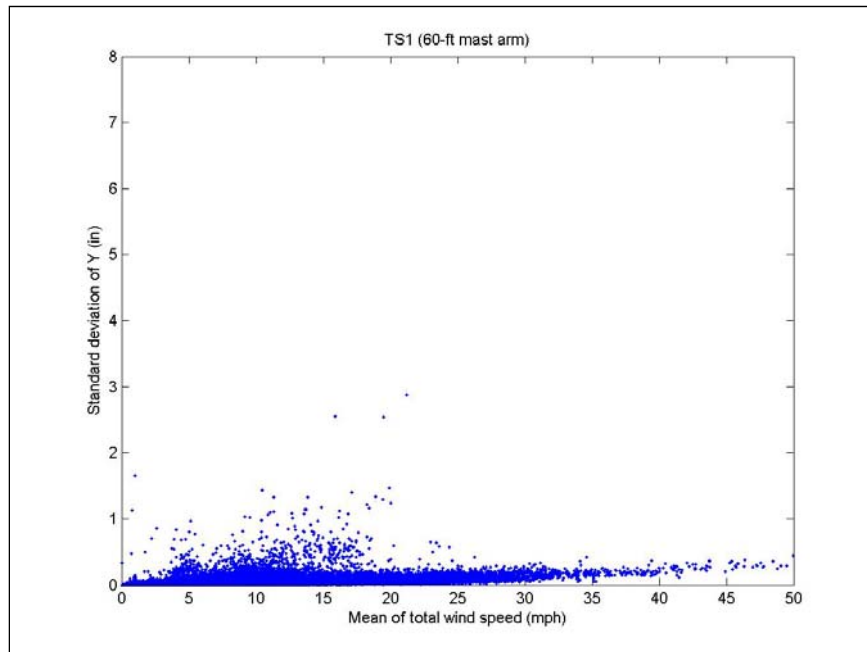
Figure B.8. Effect of total wind speed on vertical vibrations of TS1 without backplates
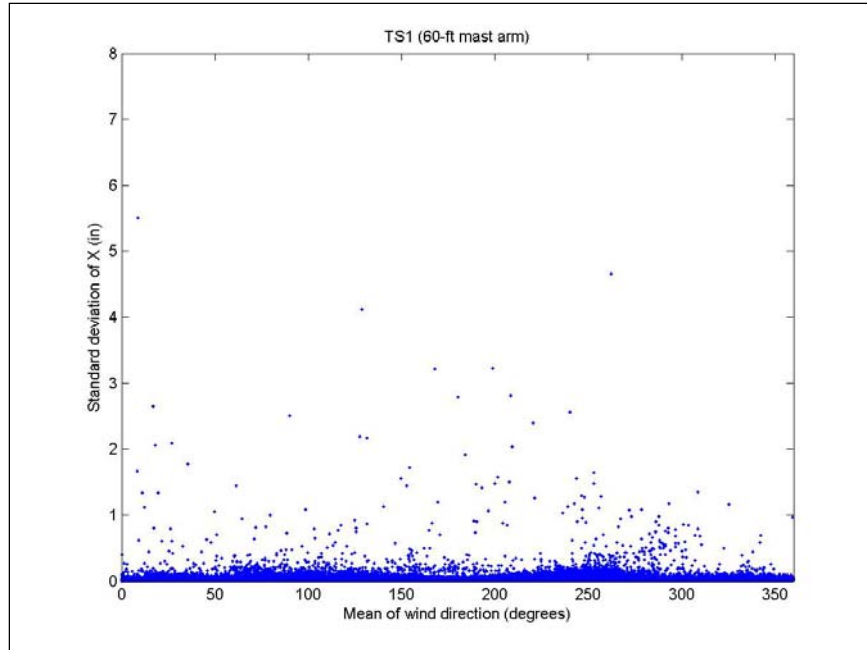
Figure B.9. Effect of wind direction on horizontal vibrations of TS1 without backplates
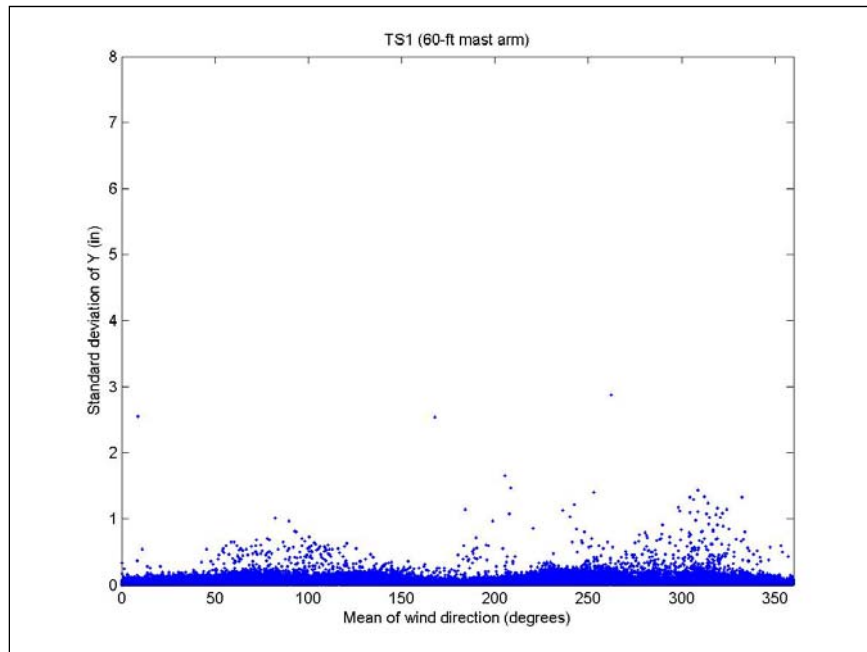
Figure B.10. Effect of wind direction on vertical vibrations of TS1 without backplates

TS2 (44-ft mast arm)

Figure B.11. Effect of u-component on horizontal vibrations of TS2 without backplates

Figure B.12. Effect of u-component on vertical vibrations of TS2 without backplates

0-4586-3

Figure B.13. Effect of v-component on horizontal vibrations of TS2 without backplates

Figure B.14. Effect of v-component on vertical vibrations of TS2 without backplates

Figure B.15. Effect of w-component on horizontal vibrations of TS2 without backplates

Figure B.16. Effect of w-component on vertical vibrations of TS2 without backplates

0-4586-3

Figure B.17. Effect of total wind speed on horizontal vibrations of TS2 without backplates

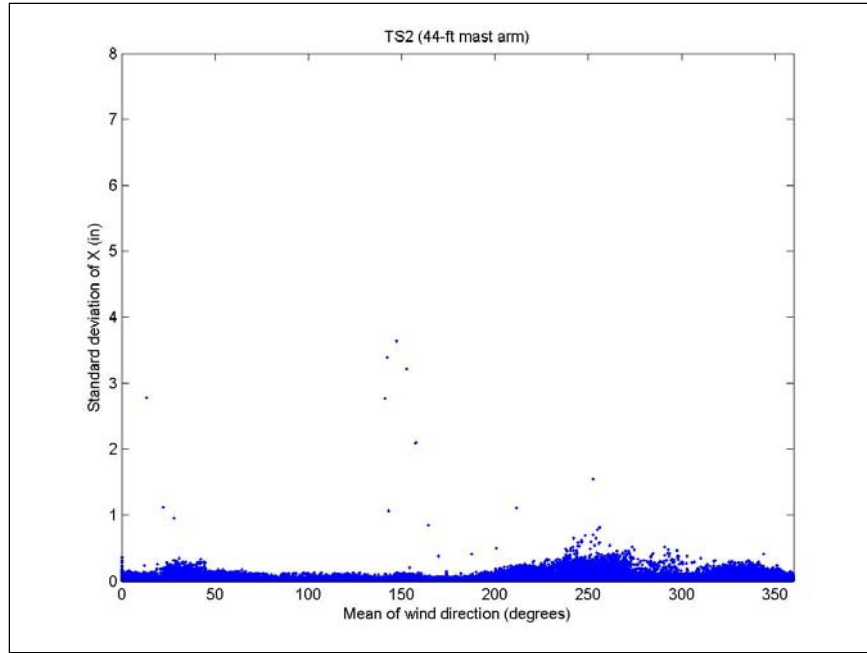Figure B.18. Effect of total wind speed on vertical vibrations of TS2 without backplates

Figure B.19. Effect of wind direction on horizontal vibrations of TS2 without backplates
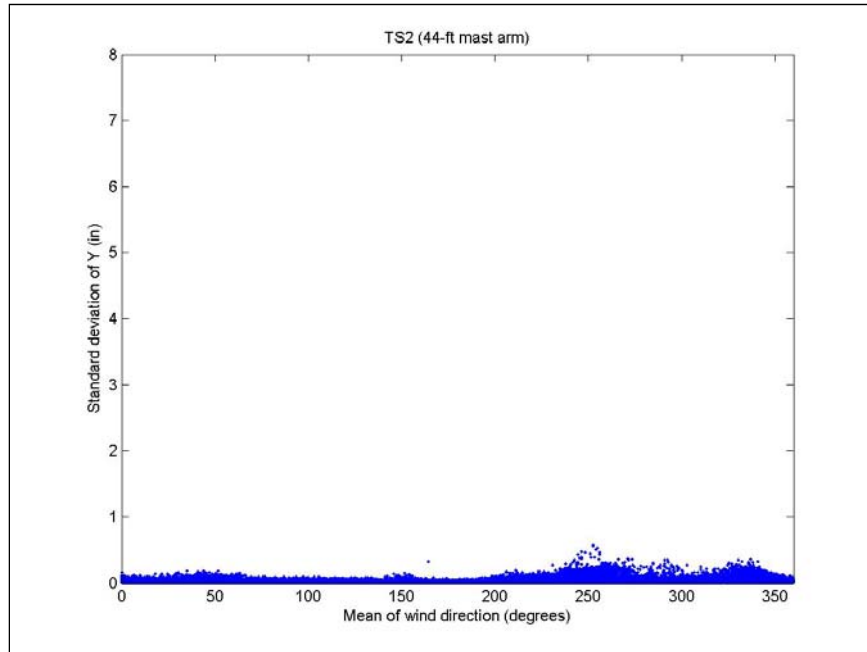

Figure B.20. Effect of wind direction on vertical vibrations of TS2 without backplates